Control of Proton-Conductive Behavior with Nanoenvironment Within Metal‑Organic Materials

Ken-ichi Otake, and Hiroshi Kitagawa**

Dr. K. Otake
Institute for Integrated Cell-Material Sciences (WPI-iCeMS), Kyoto University Institute for Advanced Study (KUIAS), Kyoto University, Yoshida-Ushinomiya-cho, Sakyo-ku, Kyoto 606-8501, Japan

Prof. H. Kitagawa
Division of Chemistry, Graduate School of Science, Kyoto University, Kitashirakawa-Oiwakecho, Sakyo-ku, Kyoto, 606-8502, Japan

E-mail: ootake.kenichi.8a@kyoto-u.ac.jp, kitagagwa@kuchem.kyoto-u.ac.jp

Keywords: Proton conductivities, metal–organic materials, porous coordination polymers, crystal structures, nanoconfinement effect

Solid-state proton-conductive materials have been of great interest for several decades due to their promising application as electrolytes in fuel cells and electrochemical devices. Metal–organic materials (MOMs) have recently been intensively investigated as a new type of proton-conductive materials. The highly crystalline nature and structural designability of MOMs make them advantageous over conventional noncrystalline proton-conductive materials—the detailed investigation of the structure–property relationship is feasible on MOM-based proton conductors. This review aims to summarize and examine the fundamental principles and various design strategies on proton-conductive MOMs, and shed light on the nanoconfinement effects as well as the importance of hydrophobicity on specific occasions, which have been often disregarded. Besides, challenges and future prospects on this field are presented.

1. Introduction

Solid materials that can conduct protons (H^+) are of increasing importance in applications such as electrolytes in sensors, batteries, and fuel cells. Investigation on proton conduction itself has a long history. Protonic current in the electrolyte was first postulated by Grotthuss in 1806 on the research on water decomposition caused by galvanic electricity.[1] This idea was acknowledged 100 years later by Danneel to explain the “abnormally” high

mobility of H^+ and OH^- in water.[2-3] Finally, solid-phase proton conduction was first suggested by Ubbelohde and Rogers in 1950 in their studies on molten sulfate salts.[4] The solid-state proton-conductive materials at the earliest stage were mainly acidic or hydrous inorganic compounds, such as hydrogen sulfate salts,[3] and later, different classes of materials gained more interest: organic polymers,[5] zeolites,[6] perovskite oxides,[7] intercalation compounds,[8] and, more recently, metal–organic materials (MOMs)[9].

The recent increasing demand for energy consumption that ascribed to the rapid urbanization and global population growth causes the rising attention to the solid-state proton-conductive materials.[10] The development of superior solid-state proton conductors is paramount for many technological innovations in high-efficiency electrochemical energy conversions. Although the phenomena of proton conduction may look simple, clarification of the true identity and development of a better conductor are both quite complicated. One classical and famous example of proton-conductive material is Nafion, which was discovered in the late 1960s and is still used today.[5] Nafion is a poly(tetrafluoroethylene)-based polymer with sulfonic acid groups in the polymer backbone. Due to its high proton conductivity as well as high thermal and mechanical property, Nafion has received considerable attention so far. Despite its long-standing history, however, the difficulty in determining the exact structure of Nafion makes it challenging to characterize the mechanism and to optimize the conduction pathways.[11] For proton to conduct efficiently, the motion of the guest molecules that work as proton conductive media is often vitally important. However, it is not easy to elucidate how the proton carriers behave and migrate in the proton conduction phenomena. Especially, confined molecules in nanoenvironment sometimes exhibit very different structural and dynamical properties than those in bulk systems.[12-14] These physicochemical effects stemming from the morphology and chemistry of nanoenvironment are denoted as “nanoconfinement effects”, which are still not fully understood. This nanoconfinement effect on proton transport recently is gaining growing interests as they are found to play an essential role in biological membrane systems as well as in mineralogy.

Recently, as a new class of proton-conductive materials, MOMs, also known as coordination polymers (CPs) and/or porous coordination polymers (PCPs), have attracted much interest due to their structural designability and uniform porosity.[15-17] MOMs are infinite coordination networks of metal ions bridged through organic ligands. Through judicious choices of structural components, the structural and physical properties of MOMs can be fine-tuned.[18-19] More importantly, thanks to the crystalline nature of MOMs, it is feasible to visualize the proton transportation pathways inside MOMs.[20] Furthermore, these

advantages of MOMs enable systematic investigation of the structure–property relationship of the proton conductivity.[21-22] Since the earliest reports of proton-conductive coordination polymers,[23-24] an exponentially increased number of MOMs have been reported, as illustrated in **Figure 1** of the report number survey. Typically, materials with proton conductivities exceeding > 10^{-3} S cm^{-1} are denoted as superprotonic conductors. To date, MOM-based superprotonic conductors with conductivities of > 10^{-2} S cm^{-1} have been developed under rational design strategies.[25] Various research groups have recently published excellent and comprehensive reviews on the recent development of MOM-based proton conductors.[9, 26-32]

This review aims to summarize the important and representative mechanistic investigations on proton-conductive MOMs. In addition, we shed light on the nanoconfinement effects on proton conduction as well as the importance of hydrophobicity on specific occasions, which have often been disregarded. Detailed discussions on measurement methods, computational works, and composite systems are beyond the scope of this review. Therefore, readers are suggested to refer to the above-cited comprehensive reviews to gain additional insight.

In the following sections, the overview of the proposed design strategy is presented, along with a brief background on proton conduction mechanisms. Then, important and representative proton-conductive MOMs are summarized, which is followed by intriguing examples of nanoconfinement effects observed in MOM materials. Finally, prospects and outlooks on MOM proton conductors are presented.

2. Proton Conduction Mechanisms

There are two general mechanisms relating to proton transport, namely, the vehicle and the Grotthuss mechanisms (**Figure 2**).[33] In the vehicle mechanism, protons migrate through a medium along with proton solvents such as H_3O^+ (hydronium cation), $H_5O_2^+$ (Zundel cation), $H_9O_4^+$ (Eigen cation), NH_4^+ (ammonium cation). This mechanism is most frequently encountered in aqueous solutions and other liquids/melts. In solids, the vehicle mechanisms are restricted to open structures to allow passage of large ions and molecules. On the other hand, the Grotthuss mechanism, or the proton-hopping mechanism, is the process where an excess proton diffuses through the hydrogen bond network of water molecules or other hydrogen-bonded molecules. Along the hydrogen bond network, the proton migrates through formation and concurrent cleavage of hydrogen bonds.[34-35] While the transport mechanism is believed to involve interconversion between these two proton solvation

structures, the details of the hopping and transport mechanism are still debated. The most plausible mechanism of proton diffusion in bulk water is believed to occur by the rapid interconversion of Eigen to Zundel to Eigen (E–Z–E) model (**Figure 3a**).[35-36] In this model, the cleavage of one hydrogen bond on the acceptor side converts an H_3O^+ cation core into $H_5O_2^+$. Then, the formation of another hydrogen bond on the donor side completes the transformation. The cleavage of one hydrogen bond is the rate-determining process, where the requiring energy would change depending on temperature, pressure, and surrounding environment. The nanoconfinement effects on proton conduction would originate from the change of these proton-hopping processes. For example, in confined water molecules in a hydrophobic nanochannel, it is predicted that a proton can diffuse by an entirely different model, known as Zundel to Zundel (Z–Z) model.[35, 37] In this model, protons can hop among neighboring sites more efficiently due to less reorientation and interconversion energy (**Figure 3b**). This model might play an important role in the efficient proton transport in hydrophobic nanochannels of biological membrane systems.[37-39] Also, in the case of narrow 2D interfaces, an almost barrierless proton transfer process is predicted.[13, 40]

In the actual proton conduction, both the vehicle and Grotthuss mechanisms are not independent and should make cooperative contributions to the conduction. From activation energy (E_a) of the proton conduction, it is possible to know which mechanism would dominantly contribute.[41-42] When the vehicle mechanism is predominantly involved in proton conduction, E_a of >0.4 eV is observed, where the transport of large ionic species requires relatively large energy. The Grotthuss mechanism takes place with less E_a (<0.4 eV) because the hydrogen-bond cleavage and its concurrent structural reorganization of hydronium ion need the energy of ~0.2 eV.

3. Design Strategy on Proton-Conductive MOMs

3.1. Basic Principle of Proton Conductivity Property

In general, conductivity, σ, can be expressed by the equation $\sigma = ne\mu$, where n is the mobile proton density, e is the elementary charge, and μ is the proton mobility. Thus, a combination of a high proton concentration and a good conduction pathway is essential for attaining high proton conductivity. To increase n in MOMs, the design of the proton source, either via an acidic moiety of the framework or acidic guests inside the pores, should be considered. The ability of molecular-level design in MOMs can be a powerful tool, for example, by decorating the crystalline structure with acidic groups. A proton source with high pK_a can enhance proton conduction because it can work as a good proton source for the

conduction. Depending on the nature of the proton sources, proton-conductive MOMs can be categorized into three types as described in the next section.[25, 30] Compared to the design strategy to increase $\boldsymbol{n}$, the design of increasing $\boldsymbol{\mu}$ is more complicated. According to thermodynamic theory,[43-44] the proton mobility can be defined as $\boldsymbol{\mu} = e\boldsymbol{D} / kT$ where $\boldsymbol{D}$ and T is a self-diffusion coefficient and temperature, respectively. $\boldsymbol{D}$ can be described as $\boldsymbol{D} = D_o \exp(-\Delta G_m / kT) = D_o \exp(\Delta S_m / k) \exp(-E_a / kT)$, where D_0 is a constant which is related to the mechanism of ionic conductivity, ΔG_m is the Gibbs energy, ΔS_m is the motional entropy and E_a is the apparent activation energy of proton conduction. By combing these relations, proton conductivity can also be described with a temperature factor as in **Equation (1):**

$$\boldsymbol{\sigma} = \frac{ne^2 D_o \exp(\frac{\Delta S_m}{k})}{kT} \exp(-\frac{\boldsymbol{E_a}}{\boldsymbol{kT}}) = \frac{\sigma_o}{kT} \exp\left(-\frac{\boldsymbol{E_a}}{\boldsymbol{kT}}\right) \quad \text{Equation (1)}$$

As seen in the equation (1), to enhance the proton conductivity of MOM materials, more charge carriers, greater motional entropy, and lower activation energy are prerequisite conditions. The motional entropy and activation energy are highly affected by the shape and environment of the proton conduction pathway. The mobility of the guests in the pore is considered to be higher in 3D diffusion rather than in 2D or 1D, because of the less collision frequency between the guests and the pore walls. Therefore, for the vehicle-type conduction, 3D network porous media may be considered a better conductor. However, this is not always the case for the actual proton conduction. Considering the Grotthuss-type conduction, the proton-hopping processes go through the cleavage and subsequent formation of hydrogen bonds, and the reorientation of proton solvents. In these processes, the mobilities of the proton or its carriers are highly affected by the pore environment and structure of hydrogen bond networks. Furthermore, as mentioned above, the nanoconfinement effect may become more evident in the low-dimensional pore, leading to enhanced carrier mobility. In consequence, a good conduction pathway is not necessarily 3D, especially in the case of Grotthuss-type diffusion. Actually, the highly mobile water molecule can also be found on the top surface or hydrophobic 1D nanochannel.[39, 45-48]

3.2. Design Strategy on Labile Proton Sources of Proton-Conductive MOMs

As described in the previous section, the existence of mobile proton sources is crucial for attaining proton conduction. Depending on the nature of the proton sources, proton-conductive MOMs can be categorized into three classifications (**Figure 4)**.[25, 30, 49]

Type I: Introduction of protonic counterion in the framework. Protonic counterions such as hydronium (H_3O^+), ammonium (NH_4^+, $MeNH_3^+$, $Me_2NH_2^+$), and hydrogen sulfate (HSO_4^-) are included during MOM synthesis or through postsynthetic counterion exchange. Protonic counterions form hydrogen bonds with the guest water or the framework itself, leading to a continuous hydrogen network with efficient proton conduction.

Type II: Intrinsic proton sources on the framework. In this type, acidic groups on the framework ligand or coordinative protonic molecules on the metal centers (H_2O, MeOH, EtOH, and imidazole) work as the proton source. The acidic group such as noncoordinated functional groups in organic ligands (e.g., -OH, -COOH, $-CONH_2$, $-SO_3H$, and $-PO_3H_2$) can work as intrinsic proton sources. The incorporation of such acidic group is achieved by two kinds of processes, i.e., employing predesigned components or postsynthetic modification. In addition, protonic framework ligands, such as hydroxyl and amine groups, which coordinated to the metal sites, could also be considered as the proton sources. Compared to the pK_a value of free ligands, the pKa of ligands coordinated to metal ions are much lower.[50] In some MOMs, the metal node of the framework contains coordinated hydroxyl and/or aqua group attached to the metal sites that are protonic.

Type III: Acid guest molecule into the pores of MOMs. The inclusion of acid molecules such as sulfonic acid, phosphoric acid, hydrochloric acid, or polyoxometalate (POMs), constitutes the simplest method of fabricating proton-conductive MOMs. However, high chemical stability against acidic guests is highly important.

Introduction of defect sites on MOMs is also a useful approach to attain a highly proton-conductive property. Depending on the nature of the defect sites, defect introduction can also be categorized into the above-mentioned classification. For example, when the defect site induces a missing linker, the coordinated protonic solvent on the induced open metal sites at the defect can be considered as the proton source (categorized as type II). It should also be noted that some good conductors can contain multiple proton sources at the same time; thus simple classification in actual cases may not be possible.

3.3. Design Strategy on Conduction Pathways of Proton-Conductive MOMs

The formation of continuous proton-hopping pathways is essential for achieving good proton conduction. However, there is no general strategy for designing a good proton

conduction pathway due to the difficulty in the planned construction of optimal hydrogen bond networks in the structures. Various factors, such as pore sizes and environment, guest species, counterions, and reaction conditions, would contribute to the formation of hydrogen bond networks. We note that the surface chemistry of MOMs is particularly important in controlling the structures and mobility of protic guest molecules within the MOMs. Also, the adequate distances and binding strengths among proton carrier sites are also critical. It is worth noting that the pK_a value of proton carrier sites should be in medium range: the sites with too low pK_a cannot accept hopping-protons effectively, while those with too high pK_a cannot release the protons. Also, one can expect efficient proton migration when the conduction pathway along sites is separated by a small energy barrier and with equal proton affinity.

In many cases of MOM proton conductors, the hydrophilic framework is advantageous for achieving high proton conduction. These hydrophilic frameworks can cooperate with or participate in forming a continuous hydrogen bond network with guest molecules (*e.g.,* water molecules), thus often leading to higher proton conductivities in such systems. Furthermore, the less hydrophobic part of the framework and the porosity of MOMs are favorable to avoid disturbing the proton-hopping pathways.[29]

However, in some specific cases, hydrophobicity of the pore environment becomes more favorable—when the proton transport occurs only among the guests in MOMs. In this case, the hydrophobicity of the framework can result in the acceleration of proton carriers due to weaker host–guest interaction. The higher mobility of these guest molecules inside the hydrophobic spaces should lead to increased vehicle-type proton transfer as well as efficient reorientation of proton carriers in the Grotthuss-type process. Although the importance of hydrophobicity on MOMs is often overlooked, it can play a vital role in making high functionality, as found in biological systems such as aquaporins and proton pumps.[37, 51-52]

Hydrophobicity can maximize this “nanoconfinement effect” of the guest molecules, as evident by the confined water molecules within a hydrophobic 1D channel or those on top surfaces.[39, 45-48] Some interesting findings on this subject are also discussed in the next section.

4. Proton-Conductive MOMs

4.1. Hydrated Proton Conductors

4.1.1. Proton Conduction in Nonporous Coordination Polymers

Nonporous-type MOMs, or coordination polymers, can show proton conductivity behavior when they have a good proton-conducting pathway, which is derived from the hydrogen bond network among the framework components. They may even exhibit anhydrous proton conductivity. In another case, because of internal or external defects, MOMs may display proton conductivity property.

1D Metal Oxalates:

In 2009, Yamada and coworkers reported a pioneering example of high proton conductivity in a crystalline MOM by studying ferrous oxalate ($Fe(ox)\cdot 2H_2O$; ox = oxalate or $C_2O_4^{2-}$).[53] Ferrous oxalate has a densely packed 1D chain structure that is composed of uninuclear ferrous sites connected by an oxalate ligand, where two water molecules are coordinated on the axial sites of Fe(II) (**Figure 5a**). In the structure, the coordinated water forms a regular 1D array of water molecules (**Figure 5b**), which was indicated to be the conduction pathway of protons. Because the coordinated water molecules at the metal centers are more acidic than free water molecules due to the Lewis acidity of the metal sites, the coordinated water can also be considered as the proton source (categorized as type II). The proton conductivity of the pelletized ferrous oxalate was 1.3×10^{-3} S cm^{-1} at 25 °C and 98% RH with an activation energy of 0.37 eV. The proton conductivities of isostructural $M(ox)\cdot 2H_2O$ (M = Fe, Mg, Ni, Co) were also evaluated, and were found to be of similarly high values.[29] They demonstrated that the Lewis acidity of the metal site affects the proton donation ability of the coordination water. Later, it was found that the proton conductivities of a single crystal of ferrous oxalate were much less than that of a pellet, indicating that protons may be transported through an aqueous phase that is formed between the particles.[54] However, at this early stage of MOF-based proton conductor development, this type of chemistry was of great importance to open up this new application of MOMs.

Prussian Blue Analogs:

As another example, the proton conduction behavior of Prussian blue analogs was reported. Prussian blue is composed of a pair of iron atoms with mixed oxidation states bridged by cyanide linkers. The structure can be varied by replacing the iron with other transition metals (so-called Prussian blue analogues; **Figure 6a**). Firstly, proton conductivity properties of vanadium–chromium and cobalt–chromium Prussian blue analogs, $Co[Cr(CN)_6]_{2/3}\cdot 4.8H_2O$ (**Co–Cr**) and $V[Cr(CN)_6]_{2/3}\cdot 4.2H_2O$ (**V–Cr**) were reported by Ohkoshi and coworkers in 2010.[55] They observed high proton conductivities of 1.2×10^{-3}

for **Co–Cr** and 1.6×10^{-3} S cm^{-1} for **V–Cr** at 293 K under 100% RH with an activation energy of 0.22 eV for **Co–Cr** and 0.19 eV for **V–Cr**, respectively. Because of the inherent vacancy sites in these compounds, the coordinated water can be considered as the proton source (type II) and the proton is carried through 3D hydrogen-bond network among the physisorbed water and the coordinated water molecules (**Figure 6b**). Interestingly, they observed that the proton conductivity of **V–Cr** increased with temperature, as expected, but with an abrupt jump in the slope of ln(σT) versus T at 313 K, which was not seen in related materials (**Figure 6c, 6d**). This temperature was found to correspond to the Curie temperature of the material—the temperature at which magnetic ordering is lost due to a change in structure. This structural change can be associated with a change in the way protons are conducted through the material. This was the first observation of an interference effect between ionic conductivity and magnetic ordering.

Proton-conductivity properties of other analogs $M[Co(CN)6]_{2/3}\cdot xH_2O$ (abbreviated as **M–Co**; where M = Ni (x = 7), Co (x = 2), Fe (x = 4), Mn (x = 1) and Cd (x = 2)) were also investigated by other groups. Conductivities at 293 K under 99% RH followed the trend of **Ni–Co** (6.9×10^{-3} S cm^{-1}) > **Fe–Co** (2.92×10^{-3} S cm^{-1}) > **Co–Co** (0.31×10^{-3} S cm^{-1}) > **Cd–Co** (0.1×10^{-3} S cm^{-1}) > **Mn–Co** (0.02×10^{-3} S cm^{-1}) with activation energies below 0.21 eV.[56] This trend actually was similar to the quantity of adsorbed water molecules rather than the Lewis acidity of the metal components, indicating that the number of defective sites would significantly affect their conducting properties. Conventionally, the arrangement of vacancies in these Perovskite Blue analogs were believed to be random. However, the recent investigation identifies a diversity of nonrandom vacancy arrangements. This new finding paves the way for better controlling efficient and anisotropic proton transport of these compounds.[57]

4.1.2. Proton Conduction in 1D Channel of MOMs

MIL-53 series:

MIL-53 is one of MOMs that has been extensively investigated by various groups.[9, 58-61] It consists of infinite chains of trans corner-sharing $AlO_4(\mu\text{-}OH)_2$ polyhedra, which are connected by 1,4-benzenedicarboxylate (bdc) linkages to form a 1D square-grid pore structure. Wide varieties of MIL-53 derivatives, [M(OH)(bdc-R)] (MIL-53(M)-R: M = Cr, Fe, Al, etc.; R = H, NH2, OH, COOH, etc.) have been reported with substitution of metal ion and/or ligands (**Figure 7a, 7b**).

Proton conductivities of MIL-53(Al) and its derivatives, MIL-53(Al)-COOH, MIL-53(Al)-OH, MIL-53(Al), and MIL-53(Al)-NH_2, were first investigated under humid conditions by Shigematsu *et al*.[61] The proton sources on these materials would be protons on the metal core as well as the additional functional groups on the bdc-derivatives that direct toward the channel. They revealed that the ionic conductivities at 298 K and 95% RH of the MIL-53 derivatives were in the order of MIL-53(Al)-COOH (2.0×10^{-6} S cm^{-1}, E_a = 0.21 eV) > MIL-53(Al)-OH (4.2×10^{-7} S cm^{-1}, E_a = 0.27 eV) > MIL-53(Al) (2.3×10^{-8} S cm^{-1}, E_a = 0.45 eV) > and MIL-53(Al)-NH_2 (2.3×10^{-9} S cm^{-1}, E_a = 0.47 eV). This order is well-correlated with the pK_a value of the functional groups (COOH < OH < H < NH_2). This is the first example in which the proton conductivity was widely controlled by substitution of ligand functional groups in an isostructural series (**Figure 7c**).

Lim and coworkers reported proton conduction mediated by NH_4^+–NH_3 conjugated system inside the pore of MIL-53(Al) derivatives.[60] Anhydrous NH_3 gas was introduced inside the pore and protonated by functional groups on the linkers, resulting in hydrogen bond networks of NH_4^+–NH_3 chain in the pore. The observed conductivity value was lower than that of H_2O-mediated conductivities due to the lower ionization character of NH_3. The NH_3-mediated proton conductor demonstrated firstly in this work paved the new material chemistry of using NH_3 as an energy carrier.

Metal–Organic Nanotubes:

Metal–organic nanotubes (MONTs) are a subclass of MOMs, and are attracting some interest in material science, owing to their intriguing architectures. MONTs have an independent 1D tubular structure and is a promising alternative of the conventional tubular-shaped compounds because the principles of reticular chemistry can be applied for MONTs. Proton conductivity properties of MONTs have been explored by several groups.

Panda and coworkers first reported proton conductivities of a series of MOMs, $(Me_2NH_2)[In(5\text{-tia})_2(H_2O)]$ (In-5TIA), $(Me_2NH_2)_2[Cd(5\text{-tia})_2(H_2O)]$ (Cd-5TIA) and $(Me_4N)[In(1,3\text{-bdc})_2]$ (In-IA), in 2012.[62] These MOMs were tubular in shape and contained countercations inside the pore (**Figure 8a, 8b, 8c**). Inner dimensions were 7.9, 8.2, and 4.9 Å, for In-5TIA, Cd-5TIA, and In-IA, respectively. Proton conductivities at 301 K under 98% RH were 5.35×10^{-5} Scm^{-1} (E_a = 0.47 eV), 3.61×10^{-3} Scm^{-1} (E_a = 0.16 eV) and 2.2×10^{-4} Scm^{-1} (E_a = 0.14 eV) for In-5TIA, Cd-5TIA and In-IA, respectively. The conductivity of Cd-5TIA was higher than those of the In complexes, due to the different number of protic (Me_2NH_2) cations per unit inside the tube, which served as the proton sources. Furthermore, the

activation energy for In-IA was relatively high, indicating that the proton conduction mechanism is close to the vehicle-type proton conduction.

In 2016, Otake and coworkers reported isostructural MOMs of homometallic $[Pt(dach)(CN)Br]_4(NO_3)_4 \cdot 4H_2O$ and its heterometallic counterpart $[Pd(dach)]_2[Pt(dach)(CN)_2Br_2]_2(NO_3)_4 \cdot 4H_2O$ with very small inner-diameter (ca. 2.0 Å) (**Figure 8d, 8e**).[63] Owing to the presence of 1D hydrogen bond networks composed of NO_3, H_2O and amine on dach ligand, they exhibit appreciable proton conductivities of 1.29×10^{-5} (E_a = 0.43 eV) and 1.54×10^{-7} Scm^{-1} (E_a = 0.54 eV), respectively, at 35°C and under 95% RH. However, the former shows 100 times higher proton conductivity than that of heterometallic one, possibly due to the lower charge modulation on the homometallic nanotube.

Just recently, superprotonic conductors with proton conductivity exceeding 10^{-2} S cm^{-1} have been reported on MONTs.[64] In 2020, Lin and coworkers reported the proton conductivity property of $[(CH_3)_2NH_2][In(cdc)(thb)] \cdot 2DMF \cdot 9.5H_2O$ (**FJU-105**) and $[(CH_3)_2NH_2][In(cdc)(H\text{-}btc)] \cdot 2DMA \cdot 11H_2O$ (**FJU-106**) (H_2cdc = 9H-carbazole-3,6-dicarboxylic acid, H_2thb = 2,5-thiophene dicarboxylic acid, H_3btc = 1,3,5-benzene tricarboxylic acid). They employed a large-sized metalloring cluster of $[In_6(cdc)_6]^{6+}$ as secondary building blocks (SBUs) that are connected to each other by a pillar linker to form a 1D tubular structure. The inner surface of **FJU-106** was functionalized by uncoordinated -COOH groups of -btc linkers, leading to a higher proton conduction than that of **FJU-105**. At 70 °C, **FJU-106** displayed the proton conduction performance of up to 1.80×10^{-2} Scm^{-1} among MONTs.

MONTs with hydrophobicity has gained a lot of interest recently, as described in the next section.

4.1.3. Proton Conduction in 2D Channels of MOMs

2D Metal oxalates:

Proton conductivity properties of a series of an isostructural oxalate-bridged 2D layered compound, $A[M_2(ox)_3] \cdot zH2O$, with varying countercation (A) and/or metal (M) species were systematically investigated by Sadakiyo and coworkers. In these MOMs, uninuclear metal ions were connected by oxalate to form honeycomb layer structures, where counterion and guest solvent molecules were located in the honeycomb void or interlayer spaces (**Figure 9a**).

Proton conductivity properties of $(NH_4)_2(H_2adp)[Zn_2(ox)_3]\cdot zH_2O$ (H_2adp = adipic acid; z = 0, 2, 3), were first reported in 2009.[25] In the crystal structure of trihydrate (z = 3), acidic molecules, H_2adp, are incorporated into the pores of the honeycomb-shaped voids (type III), and the ammonium ions and water molecules were also incorporated in the interlayer space (type I). X-ray studies revealed 2D hydrogen-bonding networks among carboxylic acidic groups, water molecules, and ammonium ions between the 2D layered frameworks (**Figure 9b**). This compound showed a superprotonic conductivity of 0.8×10^{-2} S cm^{-1} at 25 °C, 98 % RH with an activation energy of 0.63 eV. Despite the formation of the hydrogen bond networks in its structure, the observed activation energy was slightly higher than that of the typical Grotthuss-type conduction. The authors deduced that the existence of half-occupied oxygen sites of O(10) may be responsible for the relatively high activation energy because direct-jump diffusion process was required (**Figure 9c**). In addition to the trihydrate phase, this compound also transformed into two different hydrated phases: dihydrate at 10%–90% RH and anhydrate phases at 0% RH.[65] Crystal structures of these two phases were similar to each other except for the absence of water molecules. In the dihydrate, ammonium ions and water molecules were arranged alternately in the interlayer space, and it was clear that hydrogen bonds were weakened in the dihydrate compared to that in the trihydrate. Proton conductivity through the conduction pathways of the dihydrate ($< 7 \times 10^{-5}$ S cm^{-1}, 25 °C) was at least 100 times lower than that of the trihydrate. The anhydrate shows almost no ionic conductivity ($\approx 10^{-12}$ S cm^{-1}, 25 °C). The roles of ammonium ions in high proton conductivity were also studied by synthesizing a nonprotic countercation counterpart of te compound, $K_2(H_2adp)[Zn_2(ox)_3]\cdot 3H_2O$, where potassium counterions occupied the ammonium ions site without structural changes.[66] Furthermore, the effect of the hydrophilicity on the proton conductivity properties was systematically investigated by varying the cationic components in isostructural MOMs, $(NR_3(CH_2COOH))[MCr(ox)_3]\cdot zH_2O$ (R = Me, Et, or *n*-Bu; M=Mn or Fe; abbreviated as **R–MCr**).[67] In these isostructural frameworks, the hydrophilicity was attributed to the reduced hydrophobic alkyl chain length with increased space, as supported by water uptake capacity. As predicted, the revealed proton conductivities were 0.8×10^{-4} for **Me–FeCr** (65% RH), 1×10^{-7} for **Et–MnCr** (65%), 2×10^{-11} for **Bu–FeCr** (60%), and 0.8×10^{-11} S cm^{-1} for **Bu–MnCr** (60%) (**Figure 10**). These results clearly demonstrated that the control of hydrophilicity or hydrophobicity is a key factor in controlling the proton conductivity of hydrated MOFs because these properties have a strong impact on the formation and shape of hydrogen bond networks.

Okawa and coworkers investigated a series of mixed-metal 2D oxalate compounds, $A[M1M2(ox)_3]$ (A, M1, and M2 denote counteraction and two kinds of metal species) for their proton conductivity as well as magnetic properties. In 2009, they reported $(NH(prol)_3)[MCr(ox)_3]$ ($NH(prol)_3^+$ = tri(3-hydroxypropyl)ammonium; M = Mn(II), Fe(II), Co(II)), that exhibited ferromagnetic behavior at various temperatures (5.5 K for M = Mn(II) , 9.0 K for Fe(II), 10.0 K for Co(II)).[68] These compounds also exhibited high proton conductivities of approximately 10^{-4} S cm^{-1} (80% RH, 25 °C). When the nonprotoic counteraction was employed in the isostructural compound, *i.e.*, $(NBu_4)[MnCr(ox)_3]$ (NBu_4 = tetrabuhylammonium), proton conductivity was negligible (~10^{-12} S cm^{-1}). Thus, the high proton conductivity was thought to be derived from the included $(NH(prol)^3)^+$ ions and adsorbed water molecules.[69]

In 2014, Nagarkar and coworkers reported that an oxalate-based MOF material, $\{(Me_2NH_2)_3(SO_4)\}_2[Zn_2(ox)_3]$ (**Figure 11**), can conduct protons under anhydrous as well as humidified conditions: anhydrous proton conductivity of up to 1×10^{-4} S cm^{-1} at 150 °C (E_a = 0.129 eV) and hydrous superprotonic conductivity of 4.2×10^{-2} S cm^{-1} at 98% RH (E_a = 0.130 eV).[70] In its crystal structure, a hydrogen-bonded supramolecular $[(Me_2NH_2)_6SO_4]^{4+}$ cationic cluster net was interpenetrated into the $[Zn_2(ox)_3]^{2-}$ honeycomb layers. The strong and extensive hydrogen bonding in the supramolecular $[(Me_2NH_2)_3SO_4]^+_n$ net would both work as the proton source (type I) and the Grotthuss-type conduction pathways (**Figure 11c, 11d**).

4.1.4. Proton Conduction in 3D Pores of MOMs

3D Metal oxalates:

Oxalate-bridged 3D MOMs have also been studied as proton conductors by introducing cations as protonic species, such as NH_4^+ and water molecules, inside voids of anionic frameworks. With the choice of the metal species, these compounds also exhibit magnetic properties.

In 2011, Pardo and coworkers reported a proton-conductive oxalate-bridged 3D MOM, $(NH_4)_4[MnCr_2(ox)_6]\cdot 4H_2O$ where manganese(II) and chromium(II) ions were alternatively bridged by ox ions to form an infinite structure with 1D channels.[71] Protic ammonium ions were present as countercations in the channels, which could serve a role as a mobile proton source for proton conduction. This compound shows a high proton conductivity of 1.1×10^{-3} S cm^{-1} at 22 °C under 96% RH (E_a = 0.23 eV) This compound also showed

ferromagnetic ordering below T_c = 3.0 K owing to a ferromagnetic interaction between Mn(II) and Cr(III) ions through the oxalate bridge.

Polyoxametalates based MOMs:

Polyoxometalates (POMs), which are anionic oxide clusters of early transition metals, were widely used in the field of proton conduction due to its fast charge transfer capability and strong acidity.[72-73] The POMs also makes them promising as precursors to construct POM-based MOMs. The POM-based MOMs often have chemical and thermal stability as well as good electrochemical performances including proton-conductive property, thus acquiring increasing interest.[74-76]

C. Dey and coworkers first reported the proton conductivity of POM-based MOMs in 2012.[77] They reported $[Mo_5P_2O_{23}][\{Cu(phen)(H_2O)\}_3]\cdot 5H_2O$ (phen = 1,10-phenanthroline), in which two $[Mo_5P_2O_{23}]_6$ clusters are connected by a Cu(phen) unit to form a 1D chain, that were further interdigitated by π–π stacking of phen to form a 3D structure. Five non-coordinated water molecules formed a 1D water chain and worked as the proton conducting pathway. It exhibited proton conductivity of 2×10^{-5} S cm^{-1} with an activation energy of 0.23 eV at 28.8C and 98% relative humidity.

Y. Liu and cowerker's work in 2014, $H_3PW_{12}O_{40}$ was introduced into the 3D framework of HKUST-1 to construct $[Cu_{12}(btc)_8(H_2O)_{12}][H_3PW_{12}O_{40}]\cdot nH_2O$ (btc = benzene-1,3,5-tricarboxylate). The presenting MOM exhibited the proton conductivity of 4.76×10^{-5} S cm^{-1} at 90 °C 70% RH which is larger by 3 orders of magnitude compared to that of the parent HKUST-1, presumably because of the acidic POM guest in the framework.

In 2015, Y.-Q. J and coworkers reported a POM-based 3D nanotubular arrays $[Cu_3(\mu_3\text{-}OH)(H_2O)_3(atz)_3]_3[P_2W_{18}O_{62}]\cdot 14H_2O$ (Hatz = 3-Amino-1,2,4-triazole), where nanotubular $[Cu_3(\mu_3\text{-}OH)(H_2O)_3(atz)_3]_3^{2+}$ cationic frameworks were connected by $[P_2W_{18}O_{62}]^{2-}$ anions to construct 3D networks.[78] The conductivity reached 4.4×10^{-6} S cm^{-1} under 97% RH at 25 °C.

In 2016, Q. Gao and coworkers provided the first gyroidal POM-based MOM, $\{Na_7[(n\text{-}Bu)_4N]_{17}\}[Zn(P_3Mo_6O_{29})_2]_2\cdot xG$ (*n*-Bu = *n*-butyl; G = guest solvent molecules), constructed by a pair of chiral $[P_3Mo_6O_{29}]^{11-}$ enantiomers and zinc ions.[79] This compound reveals a high proton conductivity of 1.04×10^{-2} S cm^{-1} at 75% RH (80 °C) probably because of the large number of proton carriers (like water) and hydrophilic guests in the relatively large-sized POM-based 3D framework.

MIL-101 Derivatives:

In general, ionic conductivity depends on the amount and mobility of charge protons. Therefore, the encapsulation of strong acids into the porous structure of MOMs should be the simplest strategy (as described as type III in Section 2). Sulfuric acid and phosphoric acid are among the best candidates for the encapsulation due to their strong acidity and low volatility. However, the impregnation of these strong acids into MOMs is challenging because most of the MOMs cannot withstand such strongly acidic condition.

Ponomareva and coworkers achieved strong acid impregnation into a 3D MOMs, MIL-101(Cr), by soaking it into an aqueous acid solution. MIL-101(Cr) consisted of trimeric chromium(III) octahedral clusters connected by 1,4-bdc, resulting in a highly porous 3D structure. The resulting H_2SO_4@MIL-101 and H_3PO_4@MIL-101 exhibited high proton conductivities of 4.0×10^{-2} and 2.5×10^{-4} S cm^{-1} (E_a of ~ 0.42 eV) even at a low humidity condition of 20% RH. Conductivities reached 1×10^{-2} and 3×10^{-3} S cm^{-1} (E_a of ~ 0.25 eV) at 150 °C under 5 mol % H_2O in air.[80]

UiO-66 Derivatives:

Due to the high thermal and chemical stability of Zr_6-cluster node, $Zr_6(\mu_3\text{–}O)_4(\mu_3\text{–}OH)_4$, MOMs composed of such nodes are a good platform to introduce highly acidic proton sources for attaining proton conductive MOMs. Among several Zr_6-node MOMs, UiO-66, $[Zr_6(\mu_3\text{–}O)_4(\mu_3\text{–}OH)_4(1,4\text{-bdc})_6]$ (1,4-bdc = 1,4-benzendicarboxylate; UiO-66-$(OH)_4(bdc)_6$) has been most investigated probably because of the availability of their ligands and their simple preparation as well as the tunability on the ligand substitution.[81-87]

In 2015, Taylor and coworkers demonstrated a systematic defect control strategy to control the proton conduction in UiO-66. When Lewis acidic sites are exposed within UiO-66, they can act as a highly acidic proton source with coordinated water (pKa ≤ 0.3) (**Figure 12**). In this study, metal/ligand ratio was controlled through the addition of fatty acids to the synthesis, as these additives generate missing linker defects inside the MOMs. The proton conductivity increased by nearly 3 orders of magnitude to 6.79×10^{-3} S cm^{-1} ($E_a = 0.22$ eV) for $Zr_6O_4(OH)_6(bdc)_5$ compared to the pristine UiO-66 due to increases in both charge carrier concentration and mobility.[87]

Also, in 2015, Yang and coworkers reported the proton conductive properties of a series of UiO-66 derivatives by modifying H_2bdc, UiO-66-$(OH)_4$(bdc-X)$_6$ (X = SO_3H, 2COOH, NH_2, Br, H). The maximum proton conductivity varied in the following order: **UiO-**

66-SO_3H ≈ UiO-66-$(COOH)_2$ > UiO-66-NH_2 > UiO-66 > UiO-66-Br as expected from the acidity of the proton sources.[85]

In the same year in 2015, Phang and coworkers reported the postsynthetic conversion of the thiol functional group in UiO-66(−SH) into the sulfonic acid group (UiO-66(−SO_3H)) for attaining high proton. The thiol functional group in UiO-66(−SH) has a similar conductivity (2.5×10^{-5} S cm^{-1} with E_a = 0.32 eV) with that of the pristine UiO-66 (4.3×10^{-6} S cm^{-1} with E_a = 0.43 eV) at 80 °C and 90% RH, whereas UiO-66-$(SO_3H)_2$ has a higher conductivity of 8.4×10^{-2} Scm^{-1} (E_a = 0.22 eV) under the same condition. It was mainly attributed to the existence of strong Brønsted acid sites. The changes in the activation energies would be explained by the difference in the amount of water uptake at the measurement condition, which depends on the hydrophilicity of the frameworks.[84]

In 2019, Mukhopadhyay and coworkers reported two homologous MOFs, **PSM1** and **PSM2**, that were prepared by modifying **UiO-66-NH_2** through the sulfolactone reaction. **PSM1** and **PSM2** have the same structure, except that the side chain length of the -SO_3H group is different. Despite the similarity in the structure, proton conductivities of the two MOFs were fairly different: at 80 °C and 95% RH, **PSM 1** exhibited a proton conductivity of 1.64×10^{-1} S cm^{-1} (E_a = 0.11 eV), while **PSM 2** only reached 4.6×10^{-3} S cm^{-1} (E_a = 0.29 eV) (**Figure 13**). The difference in the hydrogen bond networks inside these two similar MOMs would result in a big difference in the availability of labile protons.[86]

4.2. Anhydrous Proton Conductor

Anhydrous proton conductors have potential advantages over their traditional hydrated counterparts due to their applicability at the temperature above the water boiling point. Also, such property leads to various practical benefits such as: a higher activity of the fuel cell catalyst and a decreased volume of the on-board fuel cell because a simpler cooling system is used. Thus, the discovery of potential anhydrous proton carriers is of central importance.

Anhydrous MOM proton conductors could be categorized into two types: (1) nonporous CP, where intrinsic proton-hopping pathways preexist and (2) porous CP, where hydrogen-bonding guest molcule is accommodated inside.

4.2.1. Nonporous CP-Based Anhydrous Proton Conductor

For nonporous CP to achieve anhydrous proton conduction, the existence of an intrinsic hydrogen bond network among the structural components is essential. In addition, to

achieve high proton conductivity, the hydrogen bond site should be well-ordered in the long-range and equally spaced with adequate distances to facilitate proton hopping. This type of anhydrous proton conductors is still rare.

In 2012, Umeyama and coworkers reported anhydrous intrinsic proton conduction in a nonporous $[Zn(H_2PO_4)_2(TzH)_2]$ (TzH = 1*H*-1,2,4-triazole).[88] The network consisted of mononuclear Zn^{2+} with monocoordinated orthophosphate and bridging TzH which formed parallel 2D sheets that acted as the conduction pathway. Proton hopping in MOM was promoted by rotation of phosphate ligands, which were aligned on the layers at appropriate intervals. The anhydrous proton conductivity of the network at 150 °C reached 1.2×10^{-4} S cm^{-1} (E_a = 0.60 eV) (**Figure 14**). Another nonporous CP reported by Horike and coworkers in the same year, $[Zn(HPO_4)(H_2PO_4)_2](ImH_2)_2$ (ImH = imidazole), also showed anhydrous proton conduction that reached 2.6×10^{-4} S cm^{-1} (E_a = 0.47 eV) at 130 °C.[89] The coordination networks were composed of tetrahedrally coordinated Zn^{2+} ions and two types of orthophosphates, and they formed extended 1D chain networks. The observed ImH_2^+ ions were packed close to each other due to interionic proton migration. Interestingly, these materials exhibited "plastic crystal" behavior— a long range-order disappeared while retaining a short-range disorder. The glassy states of this compound was achieved either by the melt-quench or ball milling method. The formation of glassy state of MOMs has a great potential to expand the chemistry of this area, as it contributes mechanical strength as well as processability for shaping of MOMs. In addition, the glass state may display superior properties compared to the crystalline state in some cases. For example, an amorphous glass of CP, [Cd(1,2,4-triazole)$_2$(H_2PO_4)$_2$], showed a proton conductivity that was several orders of magnitude higher than its crystalline equivalent due to the disorder and enhanced mobility of ligands in the glassy structure.[90-91]

In 2014, Tang and coworkers reported a lanthanide oxalate-based MOM, $[Eu_2(CO_3)(ox)_2(H_2O)_2]\cdot 4H_2O$, that exhibited anhydrous superprotonic conductivity reaching 2.1×10^{-3} S cm^{-1} at 150 °C (E_a = 0.47 eV).[92] The structure contains nonacoordinated Eu site, featuring coordination by five oxalates, two carbonates, and two water O atoms to form a 2D array. Eu sites in each plane were connected vertically by water ligand to form a well-ordered 1D hydrogen bonding network within the channels that are responsible for the high anhydrous proton conductivity.

In 2018, Gui and coworkers reported an anhydrous proton-conductive MOM, $(NH_4)_3[Zr(H_{2/3}PO_4)_3]$ (ZrP), which consisted of 1D zirconium phosphate anionic chains with countercations of NH^{4+}.[93] ZrP contains an inherent hydrogen-bonded infinite chain of

acid−base pairs (N−H···O−P), leading to a high anhydrous proton conductivity of 1.45×10^{-3} S cm^{-1} (E_a = 0.30 eV) at 180 °C. ZrP was further tested as electrolyte of a H_2/O_2 fuel cell, which showed a record-high electrical power density of 12 mW cm^{-2} at 180 °C among reported cells assembled from crystalline solid electrolytes.

4.2.2. Porous CP-Based Anhydrous Proton Conductor

Inclusion of guest molecules in the MOF framework is also a promising approach to obtain CP-based anhydrous proton conductors. Guest molecules can arrange in the pore to form a hydrogen bond network. As a result, the mobile proton in the ordered guest array induces proton diffusion through the hydrogen bond network.

Bureekaew and coworkers first demonstrated such anhydrous proton conductivities by encapsulating imidazole (ImH) guests into nanochannels of MOMs in 2009.[94] Imidazole guest molecules were accommodated into two types of MOMs, namely $[Al(\mu_2\text{-}OH)(1,4\text{-}ndc)]_n$ (1,4-ndc stands for1,4-naphthalenedicarboxylate) and [Al(μ2-OH)(1,4-bdc)], which have 1D channels and high thermal stability of up to 400 °C. The dynamic nature of imidazole in the pore, which was evident by both crystallographic and ^2H solid-state NMR studies, allowed for increased proton mobility at a high temperature of 120 °C. The observed conductivities at 120 °C were 2.2×10^{-5} S cm^{-1} (E_a = 0.6 eV) for ImH@$[Al(\mu2\text{-}OH)(1,4\text{-}ndc)]_n$ and 1.0×10^{-7} S cm^{-1} (E_a = 0.9 eV) for Im@[Al(μ2-OH)(1,4-bdc)], respectively. The proton conductivity of ImH@[Al(μ2-OH)(1,4-bdc)] is about 2 orders of magnitude lower than that of Im@[Al(μ2-OH)(1,4-ndc)], which was explained by the difference in the dynamic motion of the guest molecules. Nanochannels in [Al(μ2-OH)(1,4-ndc)] have a nonpolar potential surface, and polar ImH does not interact strongly with the host framework; therefore, it can move freely in this channelile, the hydrophilic nanoporous surface of [Al(μ2-OH)(1,4-bdc)] has a strong interaction that impedes the accommodated ImH mobility, resulting in a poor proton-transfer rate. The same group reported the impregnation of histamine molecules in the pore of [Al(μ2-OH)(1,4-ndc)] in 2011. The histamine@[Al(μ2-OH)(1,4-bdc)] reached a proton conductivity of 10^{-3} S cm^{-1} at 150 °C. The improvement observed with histamine@[Al(μ2-OH)(1,4-bdc)] with respect to the ImH impregnated one was explained by the higher number of protons in histamine compared to that in imidazole and the favorable packing of these protons into the nanochannels, which allows for a more efficient proton transfer.

In the same year of 2009, Hurd and coworkers demonstrated that 1*H*-1,2,4-triazole (TzH) also showed promise as an anhydrous proton conductor when loaded into a sulfonate-

lined PCP, Na_3(2,4,6-trihydroxy-1,3,5-benzenetrisulfonate) (β-PCMOF2).[95] The proton conduction in β-PCMOF2 was observed in regular 1D pores lined with sulfonate groups, which was modulated by controlled loading of 1H-1,2,4-triazole (Tz) guest molecules within the pores. Conductivity reached 5×10^{-4} S cm^{-1} at 150 °C with half loading phase of β-PCMOF2(Tz)$_x$ (x = 0.45), where the activation energy was 1.8 eV between 50 and 90 °C, and 0.34 eV between 90 and 150 °C. Lower activation energies at higher temperatures have also been observed in other solid-state ion conductors where superionic phase transitions enhance the mobility of ion vacancies.

5. Nanoconfinement Effects on Proton Conduction

5.1. Proton Conduction with 1D Hydrophobic Nanochannel

Confined water within a hydrophobic 1D channel has been predicted to have unusual structural and dynamic properties, including interesting water-cluster formation, fast water transport, and high proton conductivity.[96-98] In a hydrophobic nanochannel with a small aperture size (<2–3 nm), confined water molecules are expected to have increased mobility because of negligible interaction among pore and waters as well as the reduced number of neighboring water molecules in a restricted environment.[39, 48, 98-99] Such studies on proton dynamics in hydrophobic nanochannels are also important as biomimetics for understanding transport mechanisms in membrane proteins such as proton pumps.[47, 100-102] However, these studies have been limited to the model studies on confined water molecules in carbon nanotubes.

Otake and coworkers firstly reported a high proton conduction utilizing hydrophobic nanochannel of a nanotubular MOM.[103] [Pt(dach)(bpy)Br]$_4$(SO_4)$_4$·32H_2O (**BPY-tube**, dach: (1R, 2R)-(–)-1,2-diaminocyclohexane; bpy: 4,4′-bipyridine) was synthesized by oxidative polymerization reaction using bromine of the square [Pt(dach)(bpy)] complex (**Figure 15a, 15b**). In the crystal structure, each 1D tube was separated by sulfate anions, and this spacing left two types of channels that were either hydrophobic (channel A) or hydrophilic (channel B) in character (**Figure 15c**). Within channel A, an extended network of water molecules was arranged in alternating octamers and tetramers networks (**Figure 15d**). Water molecules in the clusters were separated from the walls of the tube by > 2.9 Å, indicating weak contact forces between the clusters and the inner surface of the nanochannel. Within channel B, water molecules formed a 1D hydrogen-bond network which included terminal dach amino groups and sulfate anions. Single-crystal impedance measurements along the channel direction revealed a high proton conduction of 1.7×10^{-2} S cm^{-1} at 328 K under 95% RH. The

conductivity value became larger with increasing relative humidity, which is indicative of the important role of the confined water molecules for the observed conductivity values. From solid-state NMR measurements, proton diffusivity was anisotropic and was reported as 2.9×10^{-11} to 1.7×10^{-12} m^2 s^{-1} through the nanochannels. The authors also suggested that the mechanism for transport was proton shuttling between water molecules located within the channel, as deduced from a combination of structural and theoretical investigation. In addition, the authors also found a continuous liquid-to-solid transition of the confined water molecules, which actually was significantly different from that of bulk water. The diameter of the channels did make a difference in water properties, and the fast proton conductivity exhibited within BPY-tube was not observed within the related compound with CN-bridging ligand, which has smaller channel diameters that were below the nanoconfinement regime (0.2 nm). The results showed strong experimental evidence of the predicted nanoconfinement effect of confined water molecules in hydrophobic nanochannels. Nanotube fabrication based on coordination chemistry can allow for systematic structural tuning of pore size, shape, and surface properties. This tunability can thus enable us to investigate the properties of confined water systematically. These findings will provide valuable structural and dynamic insights about confined molecular species in nanotubular materials as well as in biological channels.

Another demonstration of the importance of the nanoconfinement effect is the enhancement of proton conduction with the imidazole (ImH) confined in nanochannels as described in the previous section. Similar to water-mediated proton diffusion, proton transport among ImH molecules occurred via an Eigen–Zundel–Eigen scenario with the transition of imH_2^+ from an Eigen-like complex (ImH-ImH_2^+-ImH) to another, intermediated by a Zundel-like complex (ImH-H^+-ImH) (**Figure 16**).[80] However, bulk ImH (or liquid state ImH) exhibited low proton conductivity due to the short spatial/temporal correlation of proton; thus, the hydrogen bond between ImH molecules was relatively weak. By nanoconfining of ImH molecules within the 1D channel of MOMs, the highly ordered domains of ImH can form, leading to an efficient proton conduction become viable. Furthermore, nanochannel with hydrophobicity facilitated interaction among ImH molecules because the nonpolar pore surface did not interact with the polar ImH molecules. As a consequence, proton conductivities were largely enhanced in ImH confined in hydrophobic nanochannel compared to ImH confined hydrophilic nanochannel and bulk ImH. A similar tendency was also confirmed in the proton conductivities of ImH confined in Al-MOMs, CAU-11, MIL-53, MIL-53 and MIL-53-$(Me)_2$.[104] As shown in **Figure 17**, less host–guest interactions between confined ImH and nanochannel exhibited higher proton conductivities.

5.2. Proton Conduction at Surfaces or 2D Interfaces

Because the molecules on the top surface and those confined in the 2D interface interact quite differently to the surrounding environment compared to those in bulks, they can show interesting dynamic properties. For example, the existence of highly mobile water molecules at the topmost ice surface was recently clarified from combined experimental and theoretical investigation.[46] Mobile water molecules, which are bound by only two hydrogen bonds, continuously jump and roll around because of being powered by thermal vibration at the ice surface. Karim and coworkers reported an interesting work on high proton conduction of graphene oxide and its derivatives.[105] They measured the proton conductivity of bulk graphite oxide (GO'), a graphene oxide/proton hybrid (GO-H), and a graphene oxide (GO) nanosheet. The hydrophilic sites present in GO as μ_2-O, −OH, and −COOH functional groups attracted the protons, which propagated through hydrogen bond networks along the adsorbed water film. They found that the proton conductivities of GO' and GO-H under 100% humidity were $\sim 10^{-4}$ ($E_a = 0.20$ eV) and $\sim 10^{-5}$ S cm^{-1} ($E_a = 0.25$ eV), whereas that for GO was amazingly high with $\sim 10^{-2}$ S cm^{-1} ($E_a = 0.28$ eV). Theoretical investigation indicated that protons on the graphene sheet surface can hop between adjacent as well as nonadjacent hydroxyl functional groups with low energy barriers through the hydrogen bond network. Also, thin water layers confined between surfaces were predicted to exhibit most efficient proton transport through a barrierless process.[13-14, 40, 106-107] These intriguing findings would also highlight the applicability of the surface conductivity properties of MOMs that have not been well-explored.

Xu and coworkers demonstrated the proton conductivity behavior in a highly oriented MOF nanofilms, Cu-TCPP (TCPP = 5,10,15,20- Tetrakis(4-carboxyphenyl)porphyrin), which were assembled by TCPP units connected to $Cu_2(COO)_4$ paddle-wheels to produce a 3D layered structure (**Figure 18**).[108] Impedance measurements showed that this MOF nanofilm reached a conductivity of 3.2×10^{-8} S cm^{-1} at 25 °C and 40% RH, which increased to as high as 3.9×10^{-3} S cm −1 at 98% RH despite the fact that Cu-TCPP is not conductive in the bulk phase. The enhanced proton conductivity of Cu-TCPP nanofilm originated from the dangling carboxylic acid groups on its surface, which acted as Lewis acids, as well as effective proton donors.

6. Conclusions and Perspectives

Over the last few decades, MOMs have been rapidly developed as significant crystalline materials with a wide range of potential applications. Due to their chemical diversity and structural tunability, nearly 100,000 different MOMs have been reported and explored to date. This review highlights several important developments and strategies for both hydrous and anhydrous proton conductivity properties of MOMs. The tunable properties of MOMs—porosity, crystallinity, functionality, dynamics, and stability—provide a promising platform not only to investigate fundamental aspects of the proton conduction phenomena of solids but also to pursue the application to overcome the problems of existing technologies. Since the earliest examples of crystalline proton-conductive MOMs, many of superprotonic MOMs have now been realized. Some general conclusions for achieving highly proton-conductive MOMs can be drawn as follows:

(i) **Increase in carrier concentration (*n*)**. Again, as described in the Section 2, a higher concentration of proton sources and/or effective proton sources having lower pK_a values can allow for increased proton conduction.

(ii) **Formation of a continuous hydrogen bonding network**. As most of the highly proton-conductive MOMs are Grotthuss-type proton conductors, forming a good proton-hopping pathway is essential for attaining high proton conduction. In connection with this point, suitable control of the pore environment, including hydrophilicity/hydrophobicity, pore size, and the arrangement of proton sources is critical. Hydrophilic frameworks often give a good proton conductivity by facilitating the formation of continuous proton-hopping pathways. However, hydrophobic framework can be optimal by enhancing the mobility of the proton-carrying guest molecules, as described in the previous section. Also, it was found that a small change in pore size or the arrangement of proton sources sometimes drastically increases conductivity property. Thus, sensible choice of structure is important with careful consideration of the proton hopping pathways.

(iii) **Structural stability with conductive media**. For MOMs to be good proton conductors, their structural stability of MOMs is a crucial issue. Although most MOMs are not stable under water vapors due to the dissociation of the coordination bonds, the hydrated proton-conductive MOMs must withstand such operating conditions. For practical applications of the material, this point is especially important.

As for future prospects, it would remain important to strive toward higher proton conductivity property to yield better performance. Still, the realization of new strategies is of greater importance for the expansion of this field and to set MOMs apart from currently leading materials. It is crucial for MOM-based proton conductors to realize new properties, and enhance functionality, stability, and processability. We propose that the future research direction in this field includes the following consideration (**Figure 19**):

(1) **Exploration of nanoconfinement effect**. As with biological membrane protein, the surface chemistry of the interior of MOMs is important in controlling the state of the confined guest molecules within the MOMs. Variations in the chemical environment and strength of bonding within hydrophilic and hydrophobic regions of the pore can lead to very different behavior of the confined guest molecules depending on the exact interactions between the surface and the guest molecules in the nanoconfinement.[109] For example, the nanoconfinement effect in 1D hydrophobic nanochannel of water molecules can induce the interesting water-cluster formation, fast water transport, and high proton conductivity.[103, 110-112] Additional studies are required to fully explore the nature of nanoconfinement effect within MOMs and to systematically evaluate structure–property relationships.

(2) **Understanding and control of intrinsic and extrinsic proton conductivity**. Whenever powder samples are used, it is hard to remove the influence of interparticle phases, especially in hydrated conductors. Actually, some of the highly hydrous proton conduction reported may be originated from the extrinsic proton conduction at the interparticle spaces rather than intrinsic conduction. Acquiring a better understanding and control of extrinsic proton conductivity is also important for the future development of this field.[54]

(3) **Directional control in transport**. In biological systems, proton channels contribute to accomplishing numerous physiological functions through unidirectional and selective transport of protons across cell membranes.[113] However, directional control of proton transport in MOMs are still challenging and rare. As an intriguing example, in 2019, Yao and coworkers reported a chiral MOM, $[[ZnL(H_2O)]_3(H_2O)_4)]_n$ (FJU-23-H2O, H_2L = 5-triazole isophthalic acid) with switched hydrogen bond pathways within its channels. Because of its unidirectional transport of protons, this chiral MOM single crystal exhibits an ultralow set voltage (~0.2 V), a high ON/OFF ratio (~10^5), and a high rectification ratio (~10^5).[114]

(4) **Control of proton conductivity property with external stimuli**. Artificial switching of proton conductivity in MOMs may play an important role in future devices such as power generator, sensors, information storage or safety-related devices.[115-118] Controlled switchable behavior can occur by applying external stimuli, such as light irradiation, electric field, mechanical force, temperature change, or presence of a particular species. As an important demonstration, photoswitchable azobenzene moieties is incorporated as ligand of a pillared-layer type MOM.[45] Photoirradiation on the MOMs can switch between *trans* and *cis* isomers of the azobenzene moieties, leading to the response in conductivities because of the alteration of the host–guest interaction.

(5) **Shaping**. An important aspect to realize MOMs in actual applications but often overlooked is the utilization of the macroscopic form of the materials. Most studies on proton-conductive MOMs are focused on its pellet samples or single crystals, which impeded their further application in electrolyte materials as membranes in fuel cells. Thus, thin-film proton conductors constructed from pristine MOMs or membranes embedded in MOMs have also attracted considerable attention. Recently, glass-state MOMs have been investigated for proton conduction with quite different properties compared with their crystalline states.[90-91] The formation of the glass-state is also a promising approach due to its processability.

Acknowledgements

This work was supported by the ACCEL program, Japan Science and Technology Agency (JST), JPMJAC1501 and JSPS KAKENHI Grant-in-Aid for Specially Promoted Research 20H05623. KO acknowledges KAKENHI Grant-in-Aid for Early-Career Scientists (JP19K15584) for financial support.

Received: ((will be filled in by the editorial staff))
Revised: ((will be filled in by the editorial staff))
Published online: ((will be filled in by the editorial staff))

Uncategorized References

[1] S. Cukierman, *Biochimica et Biophysica Acta (BBA) - Bioenergetics* **2006**, *1757*, 876-885.
[2] V. H. Danneel, *Zeitschrift für Elektrochemie und angewandte physikalische Chemie* **1905**, *11*, 249-252.
[3] T. Norby, *Solid State Ionics* **1999**, *125*, 1-11.
[4] S. Rogers, A. Ubbelohde, *Transactions of the Faraday Society* **1950**, *46*, 1051-1061.
[5] K. A. Mauritz, R. B. Moore, *Chemical reviews* **2004**, *104*, 4535-4586.
[6] K. D. Kreuer, *Annual Review of Materials Research* **2003**, *33*, 333-359.
[7] K. D. Kreuer, W. Weppner, A. Rabenau, *Materials Research Bulletin* **1982**, *17*, 501-509.

[8] M. Casciola, U. Constantino, S. D'Amico, *Solid State Ionics* **1986**, *22*, 127-133.
[9] D.-W. Lim, H. Kitagawa, *Chemical Reviews* **2020**, *120*, 8416-8467.
[10] S. D. Ebbesen, S. H. Jensen, A. Hauch, M. B. Mogensen, *Chemical Reviews* **2014**, *114*, 10697-10734.
[11] E. Ogungbemi, O. Ijaodola, F. N. Khatib, T. Wilberforce, Z. El Hassan, J. Thompson, M. Ramadan, A. G. Olabi, *Energy* **2019**, *172*, 155-172.
[12] M. K. Tripathy, K. R. S. Chandrakumar, *Physical Chemistry Chemical Physics* **2017**, *19*, 19869-19872.
[13] U. Raviv, P. Laurat, J. Klein, *Nature* **2001**, *413*, 51-54.
[14] S. Han, M. Choi, P. Kumar, H. E. Stanley, *Nature Physics* **2010**, *6*, 685-689.
[15] S. Kitagawa, R. Kitaura, S. i. Noro, *Angewandte Chemie International Edition* **2004**, *43*, 2334-2375.
[16] H. Furukawa, K. E. Cordova, M. O'Keeffe, O. M. Yaghi, *Science* **2013**, *341*.
[17] P. Ramaswamy, N. E. Wong, G. K. Shimizu, *Chemical Society Reviews* **2014**, *43*, 5913-5932.
[18] J.-S. M. Lee, K.-i. Otake, S. Kitagawa, *Coordination Chemistry Reviews* **2020**, *421*, 213447.
[19] K.-i. Otake, Y. Cui, C. T. Buru, Z. Li, J. T. Hupp, O. K. Farha, *Journal of the American Chemical Society* **2018**, *140*, 8652-8656.
[20] F. Gandara, T. D. Bennett, *IUCrJ* **2014**, *1*, 563-570.
[21] S. Y. Kim, S. Kim, M. J. Park, *Nature Communications* **2010**, *1*, 1-7.
[22] M. F. H. S. and, W. H. Meyer, *Annual Review of Materials Research* **2003**, *33*, 233-261.
[23] S. Kanda, K. Yamashita, K. Ohkawa, *Bulletin of the Chemical Society of Japan* **1979**, *52*, 3296-3301.
[24] Y. Nagao, M. Fujishima, R. Ikeda, S. Kanda, H. Kitagawa, *Synthetic metals* **2003**, *133*, 431-432.
[25] M. Sadakiyo, T. Yamada, H. Kitagawa, *Journal of the American Chemical Society* **2009**, *131*, 9906-9907.
[26] P. Ramaswamy, N. E. Wong, G. K. Shimizu, *Chem Soc Rev* **2014**, *43*, 5913-5932.
[27] A.-L. Li, Q. Gao, J. Xu, X.-H. Bu, *Coordination Chemistry Reviews* **2017**, *344*, 54-82.
[28] Y. Y. Cai, Q. Yang, Z. Y. Zhu, Q. H. Sun, A. M. Zhu, Q. G. Zhang, Q. L. Liu, *Journal of Membrane Science* **2019**, *590*.
[29] T. Yamada, M. Sadakiyo, A. Shigematsu, H. Kitagawa, *Bulletin of the Chemical Society of Japan* **2016**, *89*, 1-10.
[30] M. Sadakiyo, T. Yamada, H. Kitagawa, *Chempluschem* **2016**, *81*, 691-701.
[31] W.-H. Li, W.-H. Deng, G.-E. Wang, G. Xu, *EnergyChem* **2020**, *2*.
[32] D. I. Kolokolov, D.-W. Lim, H. Kitagawa, *The Chemical Record*, *n/a*.
[33] K.-D. Kreuer, *Chemistry of materials* **1996**, *8*, 610-641.
[34] N. Agmon, *Chemical Physics Letters* **1995**, *244*, 456-462.
[35] O. Markovitch, N. Agmon, *The Journal of Physical Chemistry A* **2007**, *111*, 2253-2256.
[36] O. Markovitch, H. Chen, S. Izvekov, F. Paesani, G. A. Voth, N. Agmon, *The Journal of Physical Chemistry B* **2008**, *112*, 9456-9466.
[37] Z. Cao, Y. Peng, T. Yan, S. Li, A. Li, G. A. Voth, *Journal of the American Chemical Society* **2010**, *132*, 11395-11397.
[38] M. L. Brewer, U. W. Schmitt, G. A. Voth, *Biophysical Journal* **2001**, *80*, 1691-1702.
[39] C. Dellago, M. M. Naor, G. Hummer, *Physical review letters* **2003**, *90*, 105902.
[40] D. Muñoz-Santiburcio, C. Wittekindt, D. Marx, *Nature Communications* **2013**, *4*, 2349.
[41] D. K. Paul, A. Fraser, K. Karan, *Electrochemistry Communications* **2011**, *13*, 774-777.
[42] K. D. Kreuer, A. Rabenau, W. Weppner, *Angewandte Chemie International Edition in English* **1982**, *21*, 208-209.

[43] A. Bozkurt, M. Ise, K. D. Kreuer, W. H. Meyer, G. Wegner, *Solid State Ionics* **1999**, *125*, 225-233.
[44] T. Dippel, K. D. Kreuer, J. C. Lassègues, D. Rodriguez, *Solid State Ionics* **1993**, *61*, 41-46.
[45] K. Müller, J. Helfferich, F. Zhao, R. Verma, A. B. Kanj, V. Meded, D. Bléger, W. Wenzel, L. Heinke, *Advanced Materials* **2018**, *30*, 1706551.
[46] B. Weber, Y. Nagata, S. Ketzetzi, F. Tang, W. J. Smit, H. J. Bakker, E. H. G. Backus, M. Bonn, D. Bonn, *The Journal of Physical Chemistry Letters* **2018**, *9*, 2838-2842.
[47] F. Zhu, K. Schulten, *Biophysical journal* **2003**, *85*, 236-244.
[48] G. Hummer, J. C. Rasaiah, J. P. Noworyta, *Nature* **2001**, *414*, 188-190.
[49] T. Yamada, K. Otsubo, R. Makiura, H. Kitagawa, *Chemical Society Reviews* **2013**, *42*, 6655-6669.
[50] R. G. Wilkins, *Kinetics and mechanisms of reactions of transition metal complexes*, VCH Publishers, **1991**.
[51] L. C. Applegate, T. Z. Forbes, *CrystEngComm* **2020**, *22*, 3406-3418.
[52] E. Tajkhorshid, P. Nollert, M. Ø. Jensen, L. J. W. Miercke, J. Connell, R. M. Stroud, K. Schulten, *Science* **2002**, *296*, 525.
[53] T. Yamada, M. Sadakiyo, H. Kitagawa, *Journal of the American Chemical Society* **2009**, *131*, 3144-3145.
[54] S. Tominaka, A. K. Cheetham, *RSC Adv.* **2014**, *4*, 54382-54387.
[55] S.-i. Ohkoshi, K. Nakagawa, K. Tomono, K. Imoto, Y. Tsunobuchi, H. Tokoro, *Journal of the American Chemical Society* **2010**, *132*, 6620-6621.
[56] J. Vega-Moreno, A. A. Lemus-Santana, E. Reguera, A. Andrio, V. Compañ, *Electrochimica Acta* **2020**, *360*, 136959.
[57] A. Simonov, T. De Baerdemaeker, H. L. B. Boström, M. L. Ríos Gómez, H. J. Gray, D. Chernyshov, A. Bosak, H.-B. Bürgi, A. L. Goodwin, *Nature* **2020**, *578*, 256-260.
[58] V. Haigis, F.-X. Coudert, R. Vuilleumier, A. Boutin, *Physical Chemistry Chemical Physics* **2013**, *15*, 19049-19056.
[59] G. Ortiz, G. Chaplais, J.-L. Paillaud, H. Nouali, J. Patarin, J. Raya, C. Marichal, *The Journal of Physical Chemistry C* **2014**, *118*, 22021-22029.
[60] D.-W. Lim, M. Sadakiyo, H. Kitagawa, *Chemical Science* **2019**, *10*, 16-33.
[61] A. Shigematsu, T. Yamada, H. Kitagawa, *Journal of the American Chemical Society* **2011**, *133*, 2034-2036.
[62] T. Panda, T. Kundu, R. Banerjee, *Chemical Communications* **2012**, *48*, 5464-5466.
[63] K.-i. Otake, K. Otsubo, K. Sugimoto, A. Fujiwara, H. Kitagawa, *Angewandte Chemie International Edition* **2016**, *55*, 6448-6451.
[64] Q. Lin, Y. Ye, L. Liu, Z. Yao, Z. Li, L. Wang, C. Liu, Z. Zhang, S. Xiang, *Nano Research* **2020**, 1-5.
[65] M. Sadakiyo, T. Yamada, K. Honda, H. Matsui, H. Kitagawa, *Journal of the American Chemical Society* **2014**, *136*, 7701-7707.
[66] M. Sadakiyo, T. Yamada, H. Kitagawa, *Journal of the American Chemical Society* **2014**, *136*, 13166-13169.
[67] M. Sadakiyo, H. Ōkawa, A. Shigematsu, M. Ohba, T. Yamada, H. Kitagawa, *Journal of the American Chemical Society* **2012**, *134*, 5472-5475.
[68] H. Ōkawa, A. Shigematsu, M. Sadakiyo, T. Miyagawa, K. Yoneda, M. Ohba, H. Kitagawa, *Journal of the American Chemical Society* **2009**, *131*, 13516-13522.
[69] H. Ōkawa, M. Sadakiyo, T. Yamada, M. Maesato, M. Ohba, H. Kitagawa, *Journal of the American Chemical Society* **2013**, *135*, 2256-2262.
[70] S. S. Nagarkar, S. M. Unni, A. Sharma, S. Kurungot, S. K. Ghosh, *Angewandte Chemie International Edition* **2014**, *53*, 2638-2642.

[71] E. Pardo, C. Train, G. Gontard, K. Boubekeur, O. Fabelo, H. Liu, B. Dkhil, F. Lloret, K. Nakagawa, H. Tokoro, S.-i. Ohkoshi, M. Verdaguer, *Journal of the American Chemical Society* **2011**, *133*, 15328-15331.
[72] N. Osamu, K. Teruo, O. Isao, M. Yoshizo, *Chemistry Letters* **1979**, *8*, 17-18.
[73] O. Nakamura, I. Ogino, T. Kodama, *Solid State Ionics* **1981**, *3-4*, 347-351.
[74] D.-Y. Du, J.-S. Qin, S.-L. Li, Z.-M. Su, Y.-Q. Lan, *Chemical Society Reviews* **2014**, *43*, 4615-4632.
[75] D. Wang, L. Liu, J. Jiang, L. Chen, J. Zhao, *Nanoscale* **2020**, *12*, 5705-5718.
[76] B. Nohra, H. El Moll, L. M. Rodriguez Albelo, P. Mialane, J. Marrot, C. Mellot-Draznieks, M. O'Keeffe, R. Ngo Biboum, J. Lemaire, B. Keita, L. Nadjo, A. Dolbecq, *Journal of the American Chemical Society* **2011**, *133*, 13363-13374.
[77] C. Dey, T. Kundu, R. Banerjee, *Chemical Communications* **2012**, *48*, 266-268.
[78] Y.-Q. Jiao, H.-Y. Zang, X.-L. Wang, E.-L. Zhou, B.-Q. Song, C.-G. Wang, K.-Z. Shao, Z.-M. Su, *Chemical Communications* **2015**, *51*, 11313-11316.
[79] Q. Gao, X.-L. Wang, J. Xu, X.-H. Bu, *Chemistry – A European Journal* **2016**, *22*, 9082-9086.
[80] V. G. Ponomareva, K. A. Kovalenko, A. P. Chupakhin, D. N. Dybtsev, E. S. Shutova, V. P. Fedin, *Journal of the American Chemical Society* **2012**, *134*, 15640-15643.
[81] X. Chen, G. Li, *Inorganic Chemistry Frontiers* **2020**, *7*, 3765-3784.
[82] X.-M. Li, J. Liu, C. Zhao, J.-L. Zhou, L. Zhao, S.-L. Li, Y.-Q. Lan, *Journal of Materials Chemistry A* **2019**, *7*, 25165-25171.
[83] D. D. Borges, S. Devautour-Vinot, H. Jobic, J. Ollivier, F. Nouar, R. Semino, T. Devic, C. Serre, F. Paesani, G. Maurin, *Angewandte Chemie International Edition* **2016**, *55*, 3919-3924.
[84] W. J. Phang, H. Jo, W. R. Lee, J. H. Song, K. Yoo, B. Kim, C. S. Hong, *Angewandte Chemie International Edition* **2015**, *54*, 5142-5146.
[85] F. Yang, H. Huang, X. Wang, F. Li, Y. Gong, C. Zhong, J.-R. Li, *Crystal Growth & Design* **2015**, *15*, 5827-5833.
[86] S. Mukhopadhyay, J. Debgupta, C. Singh, R. Sarkar, O. Basu, S. K. Das, *ACS Applied Materials & Interfaces* **2019**, *11*, 13423-13432.
[87] J. M. Taylor, S. Dekura, R. Ikeda, H. Kitagawa, *Chemistry of Materials* **2015**, *27*, 2286-2289.
[88] D. Umeyama, S. Horike, M. Inukai, T. Itakura, S. Kitagawa, *J Am Chem Soc* **2012**, *134*, 12780-12785.
[89] S. Horike, D. Umeyama, M. Inukai, T. Itakura, S. Kitagawa, *Journal of the American Chemical Society* **2012**, *134*, 7612-7615.
[90] Y. Ohara, A. Hinokimoto, W. Chen, T. Kitao, Y. Nishiyama, Y.-l. Hong, S. Kitagawa, S. Horike, *Chemical communications* **2018**, *54*, 6859-6862.
[91] S. Horike, S. S. Nagarkar, T. Ogawa, S. Kitagawa, *Angewandte Chemie International Edition* **2020**, *59*, 6652-6664.
[92] Q. Tang, Y. Liu, S. Liu, D. He, J. Miao, X. Wang, G. Yang, Z. Shi, Z. Zheng, *Journal of the American Chemical Society* **2014**, *136*, 12444-12449.
[93] D. Gui, X. Dai, Z. Tao, T. Zheng, X. Wang, M. A. Silver, J. Shu, L. Chen, Y. Wang, T. Zhang, J. Xie, L. Zou, Y. Xia, J. Zhang, J. Zhang, L. Zhao, J. Diwu, R. Zhou, Z. Chai, S. Wang, *J Am Chem Soc* **2018**, *140*, 6146-6155.
[94] S. Bureekaew, S. Horike, M. Higuchi, M. Mizuno, T. Kawamura, D. Tanaka, N. Yanai, S. Kitagawa, *Nat Mater* **2009**, *8*, 831-836.
[95] J. A. Hurd, R. Vaidhyanathan, V. Thangadurai, C. I. Ratcliffe, I. L. Moudrakovski, G. K. Shimizu, *Nat Chem* **2009**, *1*, 705-710.
[96] K. Koga, G. Gao, H. Tanaka, X. C. Zeng, *Nature* **2001**, *412*, 802-805.

[97] Q. Li, J. Song, F. Besenbacher, M. Dong, *Accounts of chemical research* **2015**, *48*, 119-127.
[98] H. G. Park, Y. Jung, *Chemical Society Reviews* **2014**, *43*, 565-576.
[99] A. Alexiadis, S. Kassinos, *Chemical reviews* **2008**, *108*, 5014-5034.
[100] J. Geng, K. Kim, J. Zhang, A. Escalada, R. Tunuguntla, L. R. Comolli, F. I. Allen, A. V. Shnyrova, K. R. Cho, D. Munoz, *Nature* **2014**, *514*, 612-615.
[101] Y. Umena, K. Kawakami, J.-R. Shen, N. Kamiya, *Nature* **2011**, *473*, 55-60.
[102] H. Sui, B.-G. Han, J. K. Lee, P. Walian, B. K. Jap, *Nature* **2001**, *414*, 872-878.
[103] K.-i. Otake, K. Otsubo, T. Komatsu, S. Dekura, J. M. Taylor, R. Ikeda, K. Sugimoto, A. Fujiwara, C.-P. Chou, A. W. Sakti, Y. Nishimura, H. Nakai, H. Kitagawa, *Nature Communications* **2020**, *11*, 843.
[104] T. Homburg, C. Hartwig, H. Reinsch, M. Wark, N. Stock, *Dalton Transactions* **2016**, *45*, 15041-15047.
[105] M. R. Karim, K. Hatakeyama, T. Matsui, H. Takehira, T. Taniguchi, M. Koinuma, Y. Matsumoto, T. Akutagawa, T. Nakamura, S.-i. Noro, T. Yamada, H. Kitagawa, S. Hayami, *Journal of the American Chemical Society* **2013**, *135*, 8097-8100.
[106] S. Romero-Vargas Castrillón, N. Giovambattista, I. A. Aksay, P. G. Debenedetti, *The Journal of Physical Chemistry B* **2009**, *113*, 7973-7976.
[107] P. Mignon, P. Ugliengo, M. Sodupe, E. R. Hernandez, *Physical Chemistry Chemical Physics* **2010**, *12*, 688-697.
[108] G. Xu, K. Otsubo, T. Yamada, S. Sakaida, H. Kitagawa, *Journal of the American Chemical Society* **2013**, *135*, 7438-7441.
[109] C. Wang, D. Liu, W. Lin, *Journal of the American Chemical Society* **2013**, *135*, 13222-13234.
[110] V. G. Artemov, E. Uykur, P. O. Kapralov, A. Kiselev, K. Stevenson, H. Ouerdane, M. Dressel, *The Journal of Physical Chemistry Letters* **2020**, *11*, 3623-3628.
[111] K. Mochizuki, K. Koga, *Proceedings of the National Academy of Sciences* **2015**, *112*, 8221-8226.
[112] R. H. Tunuguntla, F. I. Allen, K. Kim, A. Belliveau, A. Noy, *Nature nanotechnology* **2016**, *11*, 639-644.
[113] Z. Siwy, I. D. Kosińska, A. Fuliński, C. R. Martin, *Physical Review Letters* **2005**, *94*, 048102.
[114] Z. Yao, L. Pan, L. Liu, J. Zhang, Q. Lin, Y. Ye, Z. Zhang, S. Xiang, B. Chen, *Science Advances* **2019**, *5*, eaaw4515.
[115] A. Kobayashi, S.-i. Imada, Y. Shigeta, Y. Nagao, M. Yoshida, M. Kato, *Journal of Materials Chemistry C* **2019**, *7*, 14923-14931.
[116] A. B. Kanj, A. Chandresh, A. Gerwien, S. Grosjean, S. Bräse, Y. Wang, H. Dube, L. Heinke, *Chemical Science* **2020**, *11*, 1404-1410.
[117] T.-J. M. Luo, R. Soong, E. Lan, B. Dunn, C. Montemagno, *Nature Materials* **2005**, *4*, 220-224.
[118] R. Fan, S. Huh, R. Yan, J. Arnold, P. Yang, *Nature Materials* **2008**, *7*, 303-307.

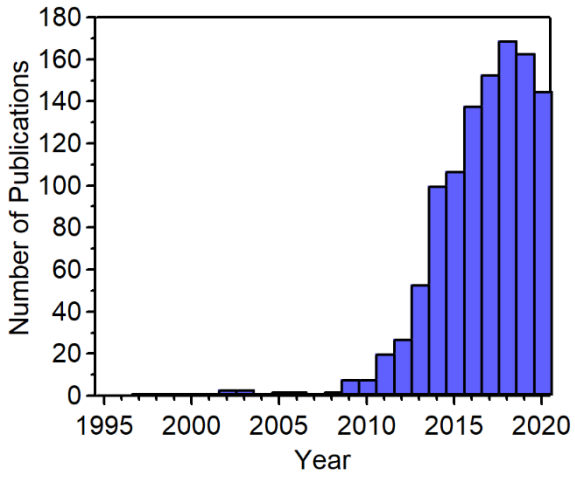

Figure 1. The number of yearly published articles containing the keywords "proton conductivity/proton conduction" and "coordination polymers/metal–organic frameworks", surveyed by Web of Science. Accessed 15th September 2020.

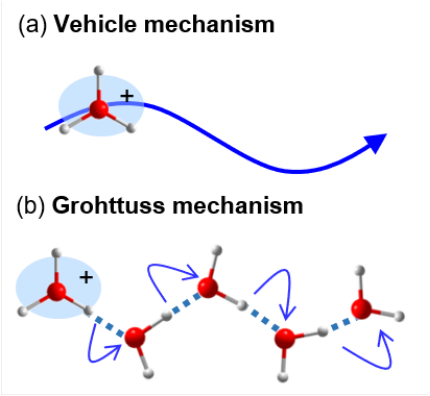

Figure 2. Schematic images of proton transport in the water medium. (a) Vehicle mechanism. (b) Grotthuss mechanism.

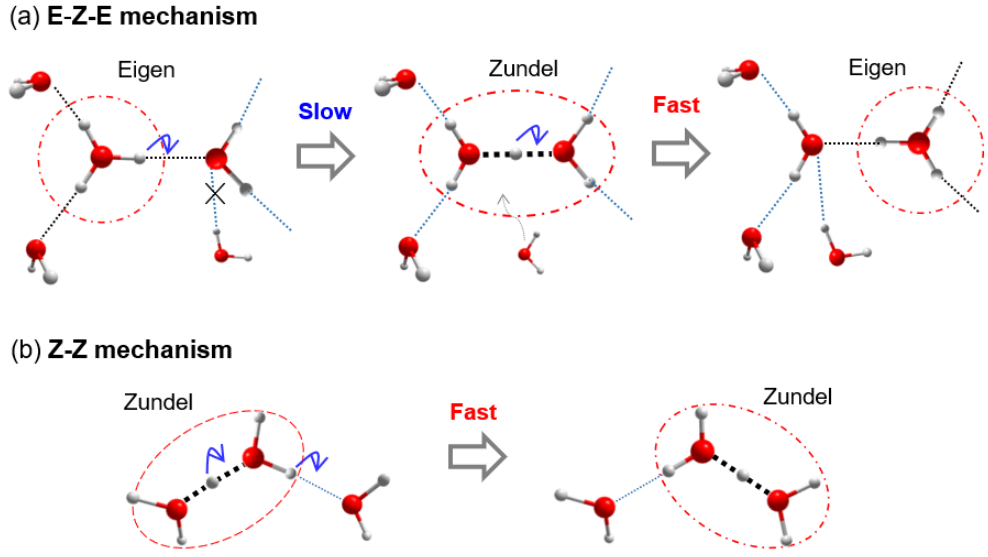

Figure 3. Schematic images of the elementary proton transport process in Grotthuss mechanism. (a) E-Z-E type mechanism. (b) Z-Z type mechanism.

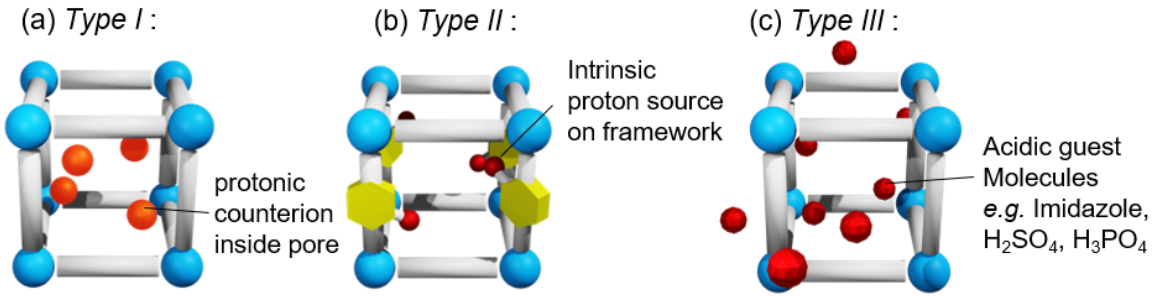

Figure 4. The design strategies to introduce mobile proton sources in MOMs (a) *type I*: counterions located in pores (b) *type II*: Intrinsic proton sources, such as acid functional groups of the organic linker or coordinated protonic solvent on the metal sites (c) *type III*: protic organic molecules or charge-neutral nonvolatile acids in the pores.

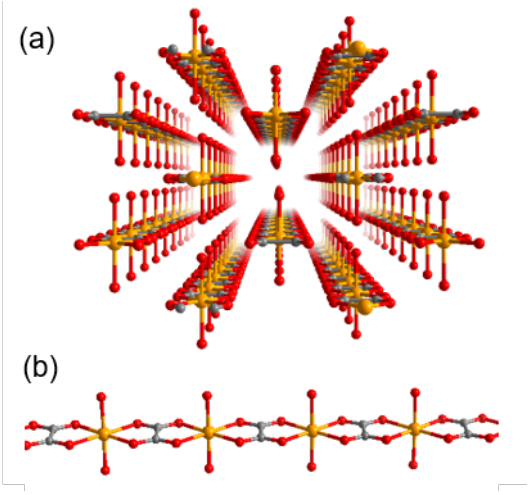

Figure 5. Crystal structures of ferrous oxalate. (a) A densely packed1D chain structure is illustrated. (b) 1D chain structure is extracted. The ordered coordinated water molecules are separated by a distance of 2.71 Å. Reproduced with permission.[53] Copyright 2009, American Chemical Society.

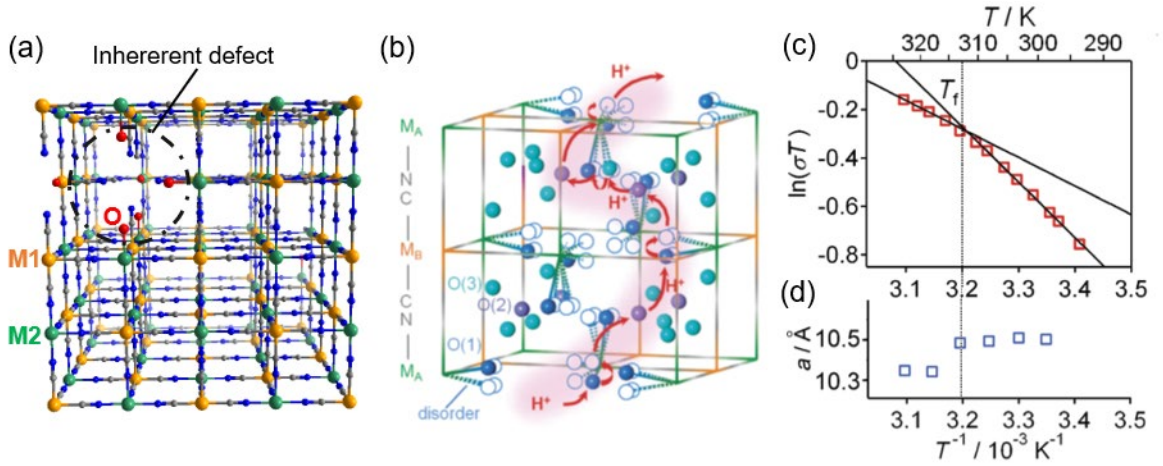

Figure 6. (a) Typical crystal structure of Perrusian blue analogs, $M2[M1(CN)_6]_{2/3}$. M1and M2 denote two metal species. M1, M2, C, N, O are represented by orange, green, gray, blue, and red spheres, respectively. (b) A possible pathway of the proton transfer in **V–Cr** through hydrogen bonds between ligand water and coordinated water molecules. (c) Arrhenius plot of the proton conductivity of **V–Cr**. (d) Temperature dependence of lattice constant of **V–Cr**. They contain inherent defects as illustrated by the dotted circle. Reproduced with permission.[55] Copyright 2010, American Chemical Society.

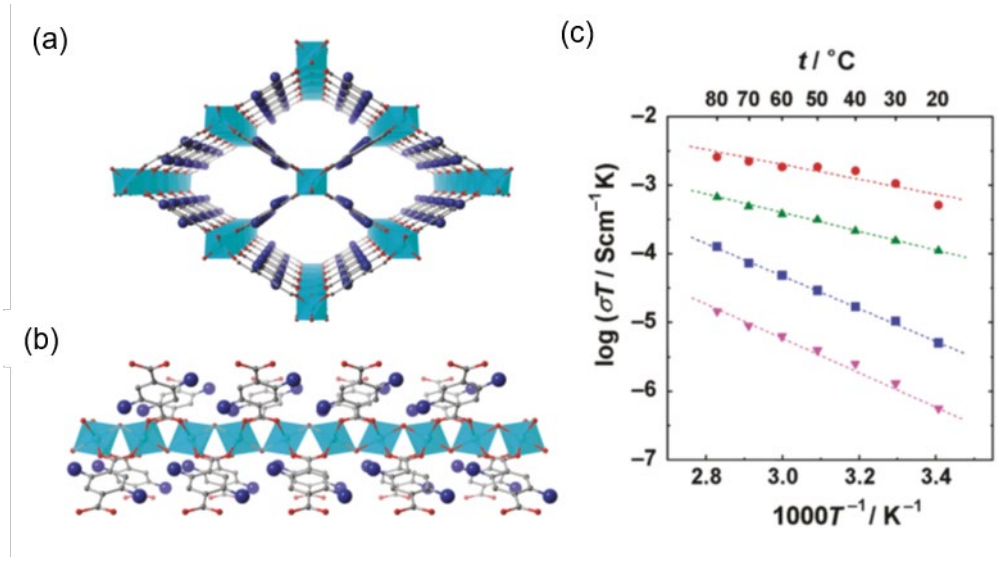

Figure 7. Crystal structures of MIL-53 deliveries. (a) Chains of corner-sharing $MO_4(OH)_2$. (b) The structure along the channel axis. Al or Fe, C, O, and H are represented as light-blue, gray, red, and blue, respectively. The blue atoms show functional groups ($-NH_2$, $-OH$, or $-COOH$). (c) Arrhenius plots of the proton conductivities of MIL-53(Al)-COOH (blue square), MIL-53(Al)-OH (pink triangle), MIL-53(Al) (green triangle), and MIL-53(Al)-NH_2 (red circle) under 95% RH conditions. Least-squares fits are shown as dotted lines. Reproduced with permission.[61] Copyright 2011, American Chemical Society.

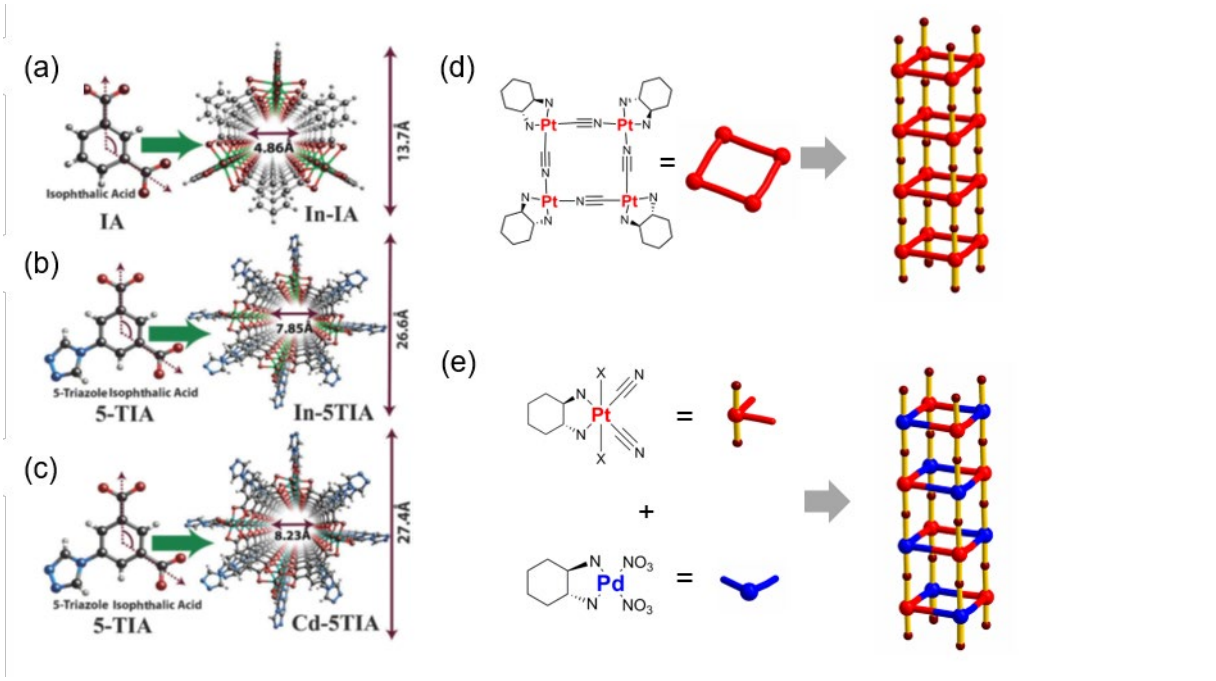

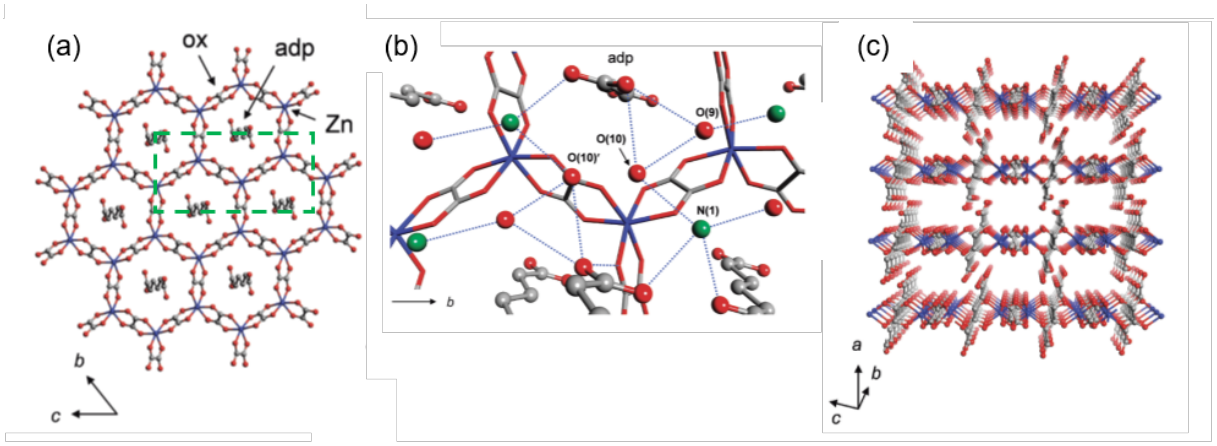

Figure 9. Crystal structures of **1**. (a) Honeycomb layer structure of **1**. (b) Expanded structure in the area colored in green in (a). Hydrogen-bond arrangements of −COOH, H_2O, and NH_4^+ in the interlayer are depicted. Hydrogen bonds are shown as blue dotted lines. (c) Perspective view along the *b*-axis. Guest molecules are omitted. Zn, C, O, N atoms are represented by red, green, gray, and blue colors, respectively. Reproduced with permission.[25] Copyright 2009, American Chemical Society.

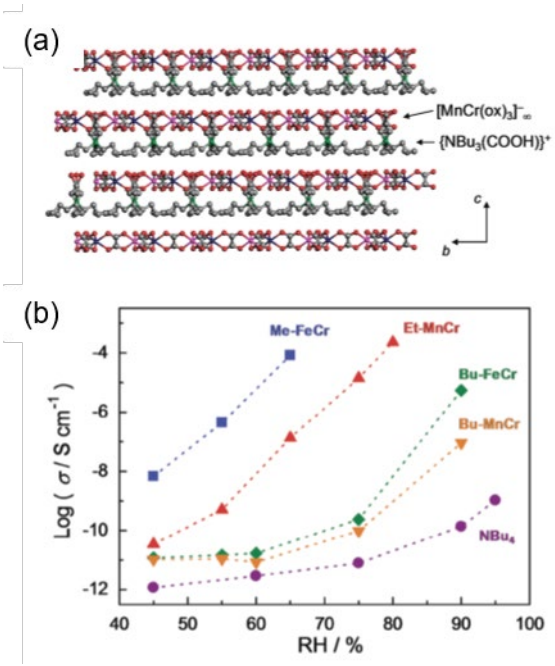

Figure 10. (b) Humidity dependence of the proton conductivity at 298 K. The blue, red, green, orange, and purple colors correspond to the proton conductivity of **Me-FeCr**, **Et-MnCr**, **Bu-FeCr**, **Bu-MnCr**, and **NBu4**, respectively. Reproduced with permission.[67] Copyright 2012, American Chemical Society.

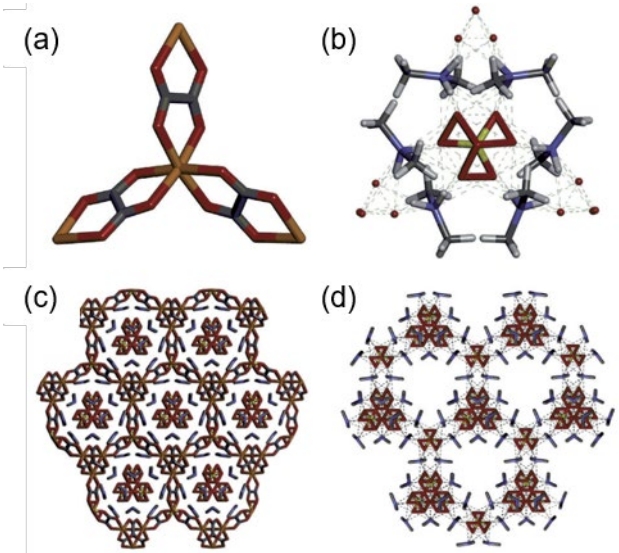

Figure 11. Crystal structures of $\{[(Me_2NH_2)_3(SO_4)]_2[Zn_2(ox)_3]\}_n$ (a) The tris-chelated D_3-symmetric $[Zn_2(ox)_3]_2$ subunit (b) 3D supramolecular $[(Me_2NH_2)_3SO_4]^+_n$ net formed by hydrogen bonding between dimethyl ammonium cations and sulfate anions. (c) Packing structure of the MOM (d) Hydrogen bond interactions between dimethyl ammonium cations and sulfate anions in the MOM. Zn, C, N, O, S atoms are represented by orange, gray, blue, red, and yellow colors, respectively. Reproduced with permission.[70] Copyright 2013, John Wiley and Sons.

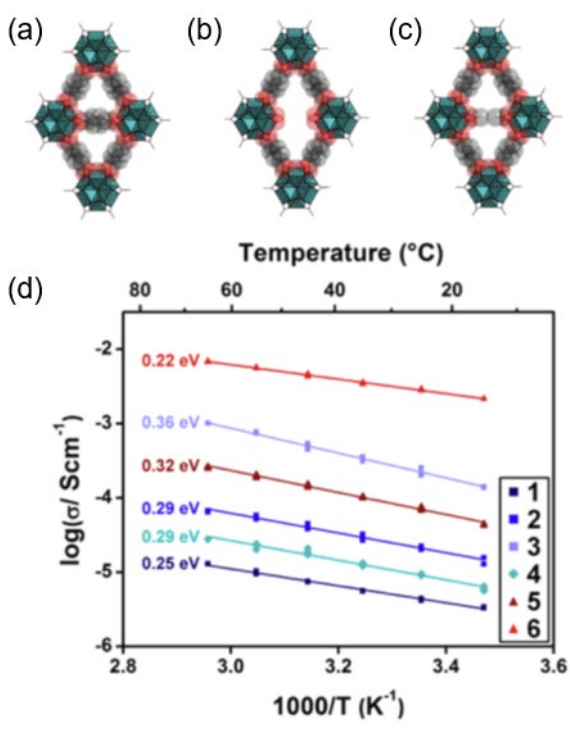

Figure 12. (a–c) Schematic views of ligand defects in UiO-66, showing the increase in pore size. (a) defect-free UiO-66 (b) terephthalates are missing on the Zr-clusters, where hydroxyl groups are coordinated on the metal sites (c) terephthalates are missing on the Zr-clusters, where acetate are coordinated on the metal sites. (d) Defect control of proton conductivity of UiO-66. Reproduced with permission.[87] Copyright 2015, American Chemical Society.

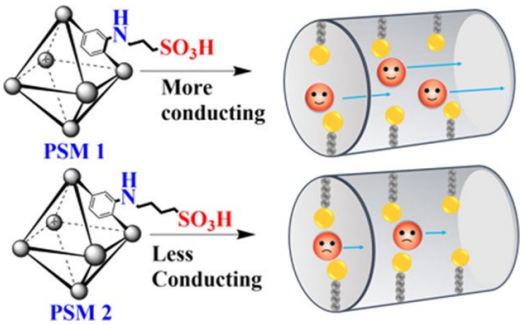

Figure 13. Schematic illustration of structures and proton conduction in **PSM1** and **PSM2**. UiO-66-NH_2 were treated with 1,3-propane sultone and 1,4-butane sultone to obtain **PSM1** and **PSM2**, respectively. Reproduced with permission.[86] Copyright 2019, American Chemical Society.

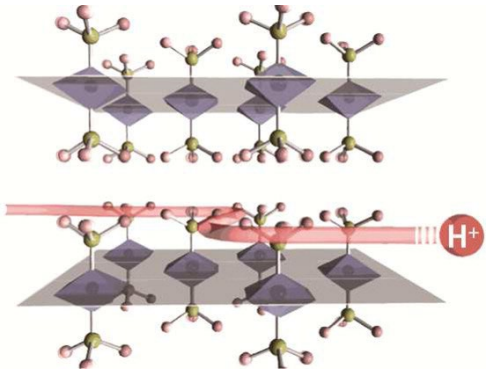

Figure 14. Intrinsic proton conduction in a nonporous MOM. Proton hopping was promoted by rotation of phosphate ligands. Reproduced with permission.[88] Copyright 2012, American Chemical Society.

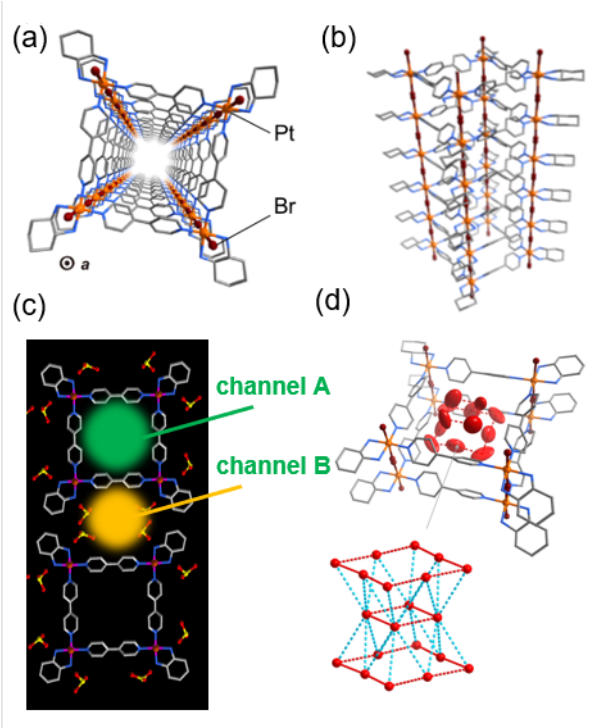

Figure 15. Crystal structures of **BPY-tube**. (a) and (b) The four-legged tubular structure of BPY-tube is illustrated. (c) The packing structure of BPY-tube. Channels A and B are highlighted by light green and orange circles, respectively. Water molecules are omitted for clarity. (d) Tetramer and octamer-like water cluster within the hydrophobic channel of **BPY-tube**. Pt, Br, S, C, and N atoms are represented by orange, brown, yellow, gray, and blue spheres, respectively. Reproduced with permission.[103] Copyright 2020 Nature Publishing Group.

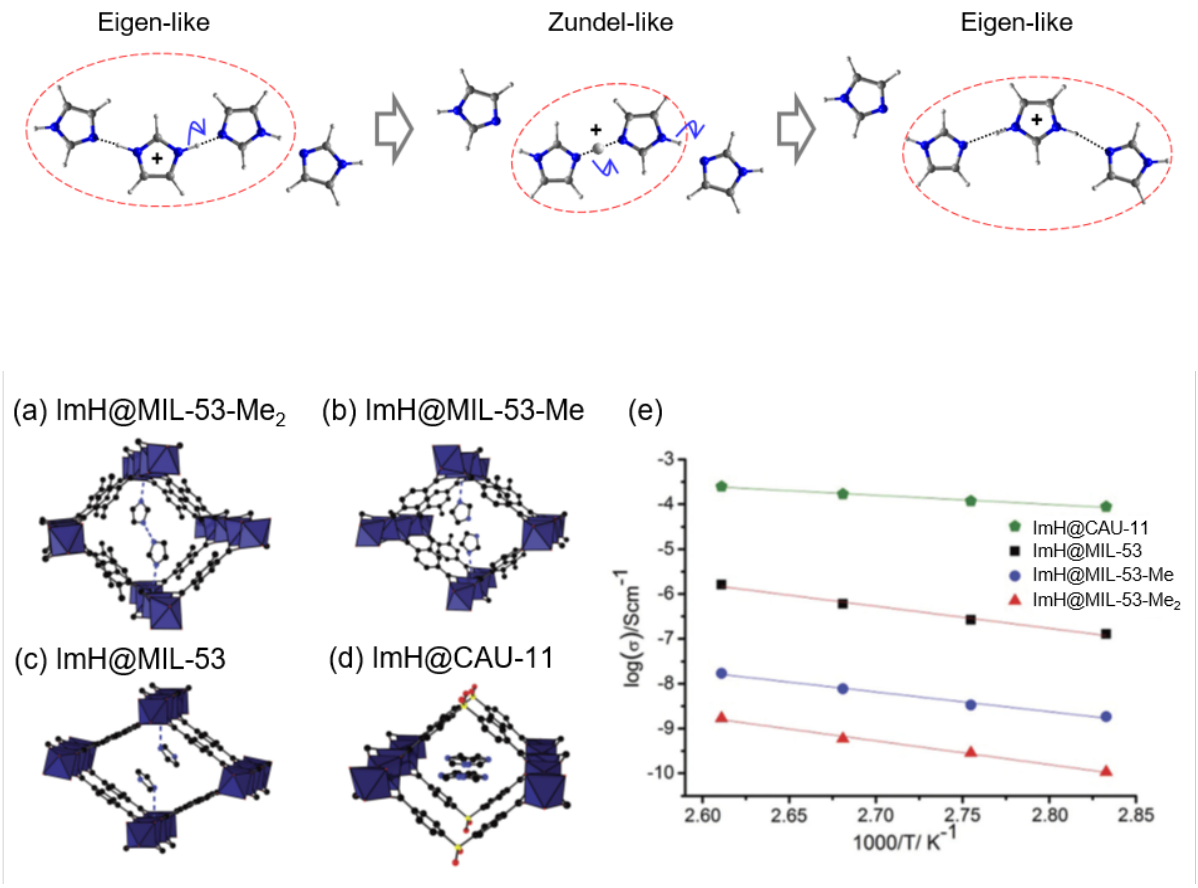

Figure 17. (a–d) crystal structures of ImH confined Al-based MOMs, ImH@MIL-53-Me_2, ImH@MIL-53-Me, ImH@MIL-53, and ImH@CAU-11 (e) the Arrhenius plots of their proton conductivities. AlO_6 polyhedra are shown in dark blue, carbon atoms in black and nitrogen atoms in light blue. The potential hydrogen bonds are shown as dashed blue lines. Reproduced with permission.[104] Copyright 2016, Royal Society of Chemisty.

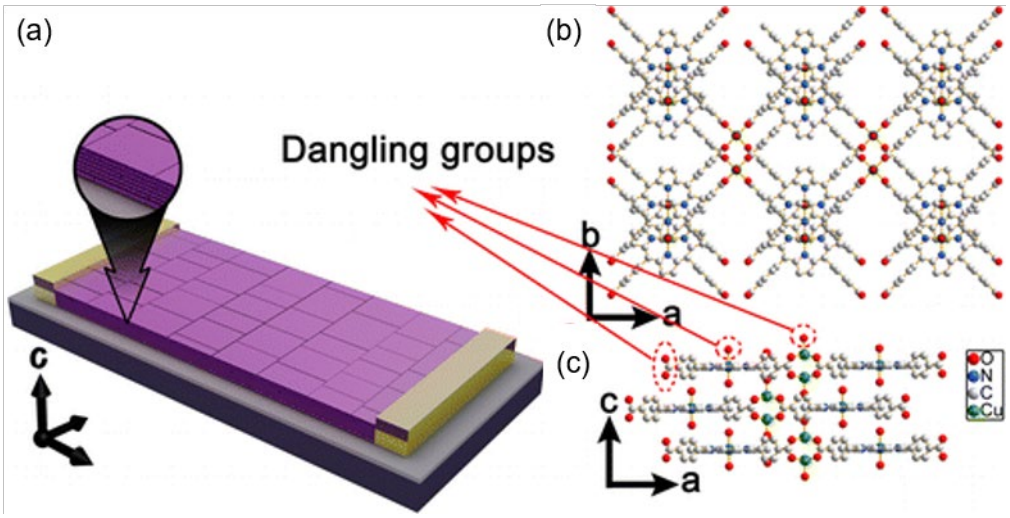

Figure 18. (a) Schematic illustration of the MOM nanofilm based device. (b) and (c) Simulated crystal structures of MOM nanofilm. Reproduced with permission.[108] Copyright 2013, American Chemical Society.

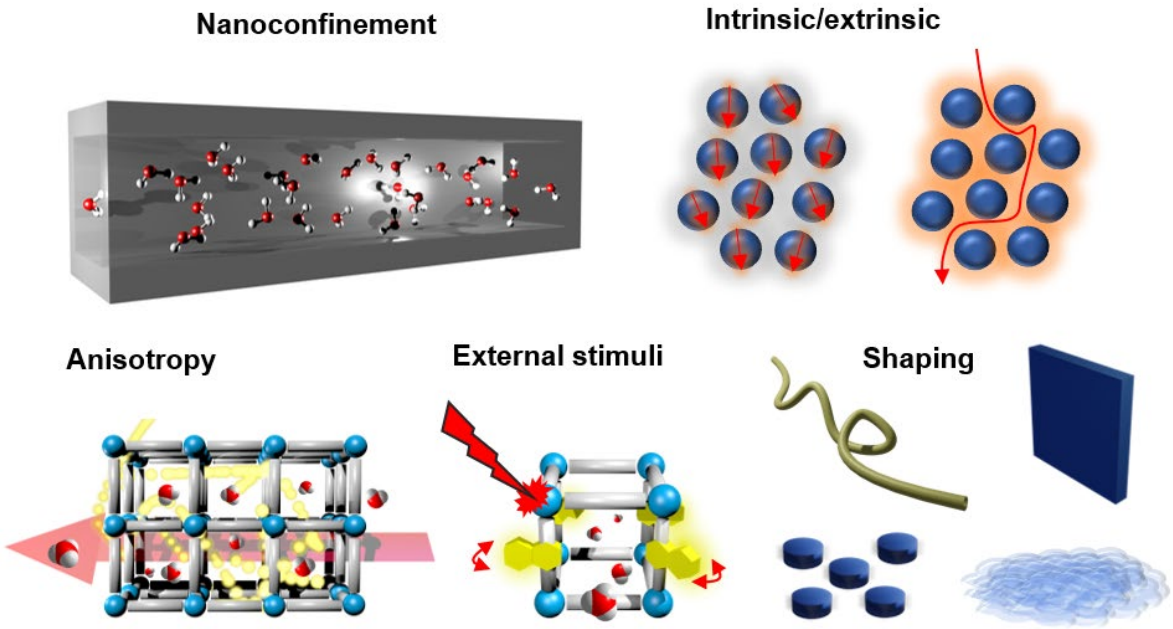

Ken-ichi Otake received his Ph.D. from the Department of chemistry, the faculty of science, Kyoto University in 2016 under the supervision of Professor Hiroshi Kitagawa. After two years of research as a postdoctoral researcher at Northwestern University under the supervision of Professor Joseph T. Hupp and Omar K. Farha, he became an assistant professor at the institute of Cell-Materials Sciences, Kyoto University in 2018. His research interests cover coordination chemistry, solid-state chemistry, and catalysts.

Hiroshi Kitagawa finished his Ph.D. at Kyoto University in 1991. After working as an Assistant Professor at IMS and JAIST, he was appointed as an Associate Professor at the University of Tsukuba in 2000. He became a Professor at Kyushu University in 2003 and at Kyoto University in 2009. He is engaged at the JST as a Research Director of ACCEL, a Director of the network-type research institution “Science and Creation of Innovative Catalysts, PRESTO” and Program Officer, Materials Science Panel, Fusion Oriented Research for Disruptive Science and Technology (FOREST). He is now President of Japan Society of Coordination Chemistry.

The high crystallinity and designability of Metal–Organic Materials (MOMs) make them advantageous over conventional noncrystalline counterparts. This review summarizes and examines the fundamental principles and various design strategies of proton-conductive MOMs, and shed light on the nanoconfinement effects and the importance of hydrophobicity on specific occasions, which have been often disregarded. Besides, challenges and future prospects are presented.

K. Otake*, H. Kitagawa*

Control of Proton Conductive Behavior with Nanoenvironment within Metal‑Organic Materials